# INFORMATION TO USERS

This manuscript has been reproduced from the microfilm master. UMI films the text directly from the original or copy submitted. Thus, some thesis and dissertation copies are in typewriter face, while others may be from any type of computer printer.

**The quality of this reproduction is dependent upon the quality of the copy submitted.** Broken or indistinct print, colored or poor quality illustrations and photographs, print bleedthrough, substandard margins, and improper alignment can adversely affect reproduction.

In the unlikely event that the author did not send UMI a complete manuscript and there are missing pages, these will be noted. Also, if unauthorized copyright material had to be removed, a note will indicate the deletion.

Oversize materials (e.g., maps, drawings, charts) are reproduced by sectioning the original, beginning at the upper left-hand corner and continuing from left to right in equal sections with small overlaps.

Photographs included in the original manuscript have been reproduced xerographically in this copy. Higher quality 6" x 9" black and white photographic prints are available for any photographs or illustrations appearing in this copy for an additional charge. Contact UMI directly to order.

ProQuest Information and Learning
300 North Zeeb Road, Ann Arbor, MI 48106-1346 USA
800-521-0600

# DIFFUSE LIGHT CORRECTION FOR FIELD REFLECTANCE MEASUREMENTS

by

John Henry LaMarr

---

A Dissertation Submitted to the Faculty of the

COMMITTEE ON OPTICAL SCIENCES (GRADUATE)

In Partial Fulfillment of the Requirements
For the Degree of

DOCTOR OF PHILOSOPHY

In the Graduate College

THE UNIVERSITY OF ARIZONA

2001

**THE UNIVERSITY OF ARIZONA ®**
**GRADUATE COLLEGE**

**As members of the Final Examination Committee, we certify that we have read the dissertation prepared by** John LaMarr

**entitled** Diffuse Light Correction for Field Reflectance Measurements

**and recommend that it be accepted as fulfilling the dissertation requirement for the Degree of** Doctor of Philosophy

| | |
|---|---|
| Kurt Thome | Oct 9, 2000 **Date** |
| Arvind Marathay | Oct 9, 00 **Date** |
| Stuart Biggar | Oct 9, 2000 **Date** |
| | **Date** |
| | **Date** |

**Final approval and acceptance of this dissertation is contingent upon the candidate's submission of the final copy of the dissertation to the Graduate College.**

**I hereby certify that I have read this dissertation prepared under my direction and recommend that it be accepted as fulfilling the dissertation requirement.**

**Dissertation Director** , Kurt Thome — Nov 20, 2001 **Date**

## STATEMENT BY AUTHOR

This dissertation has been submitted in partial fulfillment of requirements for an advance degree at the University of Arizona and is deposited in the University Library to be made available to borrowers under rules of the Library.

Brief quotations from this dissertation are allowable without special permission, provided that accurate acknowledgment of source is made. Requests for permission for extended quotation from or reproduction of this manuscript in whole or in part may be granted by the head of the major department or the Dean of the Graduate College when in his or her judgement the proposed use of the material is in the interests of scholarship. In all other instances, however, permission must be obtained from the author.

SIGNED: 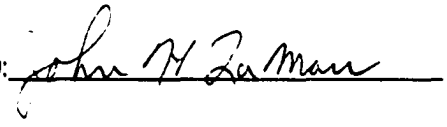

## ACKNOWLEDGMENTS

I would like to thank my advisor, Kurt Thome, for his direction and patience throughout my time with the Remote Sensing Group. I also wish to express my appreciation for his help in processing and collecting the data used in this research. I am fortunate to have worked for and with him.

I would also like to thank the members of my committee, Stu Biggar and Arvind Marathay. This work has benefitted from their comments and suggestions.

My coworkers have been a great help to me. I would like to thank Emily Whittington and Rob Kingston for their help in collecting data. I would also like to acknowledge Nik Anderson, Michell Kuester, Prabal Nandy, Ernie Nelson, Sheryl Recker, and Chip Smith for their help and support.

Finally, I would like to thank my family for encouraging me and believing in me throughout this process. I especially want to thank my wife, Ruth, for giving me pep talks when I needed it, for keeping our home running smoothly, and for helping to with one of the experiments presented here.

TABLE OF CONTENTS

TABLE OF CONTENTS - Continued

Page

TABLE OF CONTENTS - Continued

Page

# LIST OF FIGURES

Page

LIST OF FIGURES - Continued

Page

LIST OF FIGURES - Continued

Page

# LIST OF TABLES

Page

## ABSTRACT

The Remote Sensing Group of the Optical Sciences Center at the University of Arizona performs absolute radiometric calibration of Earth-viewing sensors using vicarious methods. The reflectance and irradiance -based methods require the nadir-view reflectance of a calibration site at sensor overpass. Errors in these reflectance data contribute directly to errors in the retrieved at-sensor radiance, and therefore errors in the calibration.

This research addresses two areas of improvement for the reflectance retrieval. The discreet laboratory data of the reference panel is spectrally interpolated using the measured hemispherical reflectance rather than a polynomial fit. This interpolation better fits an absorption feature of the reference material near 2200 nm.

The desired reflectance is due to the directly-transmitted solar irradiance, but field measurements also include irradiance due to diffuse light. Non-lambertian properties of the reference and surface cause the ratio of the reflected total radiances to differ from the ratio of the reflected solar radiances. This difference can be corrected using additional field measurements, shaded-surface/shaded-reference, output from a radiative transfer code, RTC-only, or a combination of both, shaded-reference. For the shaded-reference and RTC-only methods the shape of the bi-directional reflectance factor of the surface must be known to better than 10% to maintain a 2% accuracy for the retrievals, while the shaded-surface/shaded-reference method does not use the surface BRF.

All three methods were applied to measurements of calibrated reflectance tarpaulins, and the shaded-reference and RTC-only methods were applied to measurements of Ivanpah Playa. These data demonstrate that the shaded-surface/shaded-reference and RTC-only

methods improve the surface reflectance retrieval, while the shaded-reference method is too sensitive to variations between the actual and modeled diffuse sky irradiance to be useful.

This research represents significant improvements in the calculation of surface reflectance for vicarious calibration. The hemispherical reflectance interpolation will reduce uncertainties in the short wave infrared by 1%, and the diffuse corrections will reduce the errors in blue by 2% in some cases.

# CHAPTER 1

# INTRODUCTION

Absolute radiometric calibration is the process of determining the relationship between a sensor's raw output (digital counts, voltage, needle position, etc.) and the physical quantity being measured (power, speed, angle). In the case of remote sensing instruments, the most common calibration conversion is from digital number (DN) to spectral radiance, $L_\lambda$ ($W\ m^{-2}\ sr^{-1}\ \mu m^{-1}$). There are three distinct types of calibrations: preflight, on-board in flight, and vicarious.

The first, pre-flight calibration, refers to the approach where the sensor is calibrated before it is launched. This calibration can be done in the laboratory in a controlled environment, and can be referenced to primary calibration sources from national laboratories. One common method of preflight calibration begins by transferring the calibration of a primary standard (such as a variable temperature blackbody calibrated by the Japanese National Research Laboratory of Metrology (NRLM)) to a spherical integrating source (SIS) (Ono et al., 1996). The SIS is a fairly uniform radiance source which can be set to various radiance levels by adjusting the number of lamps in use or by changing the electrical power input. For a linear detector the different radiance level data can be fit to a solution of the form DN=AL+B, where B is the dark signal of the sensor and A is the proportionality constant (Dinguirard and Slater, 1999). As an alternate source, the sun has been used with a diffuser panel to calibrate sensors such as SeaWiFS (Biggar et al., 1993; Biggar et al., 1997) and ScaRaB (Dinguirard et al., 1998; Mueller et al., 1996), and this has the advantage

of supplying a source that is spectrally similar to that encountered in the operation of the sensor.

After the sensor is launched, several factors such as reflectance changes in mirrors can lead to changes in the system response (Hovis et al., 1985). Therefore it is important to have a method to calibrate the sensor in flight as well as pre-flight. One solution is the second type of satellite calibration, on-board calibrators, such as lamps (Landsat 5 TM, Thome et al., 1997) or solar diffusers (MISR, Bruegge et al., 1995). In the case of a lamp, the calibrator is located inside the satellite, and it is possible for the detector to view the calibrated source on demand. For example, the Landsat Thematic Mapper sensors view the calibrated lamp at the end of each scan line (Thome et al., 1997). One difficulty with lamps is that due to their location within the satellite platform, the calibration performed often does not include the entire optical path, and in many cases does not illuminate the entire aperture. In these cases, changes in the omitted optical elements may be erroneously interpreted as changes in the scene radiance. Similarly, changes in the relative calibration of the detector elements will be misinterpreted in the case where the aperture is not fully illuminated. On-board calibrators are in many cases calibrated originally using the pre-flight calibration as a reference, and can therefore never attain accuracies better than the pre-flight. For instance, the Advanced Spaceborne Thermal Emission and Reflection Radiometer (ASTER) has pre-flight calibration accuracies of ±2.2% and ±3.0% in the Visible and Near Infra Red (VNIR) and the Short Wave Infra Red (SWIR) respectively, and a total accuracy using the on-board calibrators of ±3.8% for both regions (Ono et al., 1996).

As with the pre-flight lamp based calibrations, the spectral distribution of the lamp is very different from the solar curve (Dinguirard and Slater, 1999). A solar diffuser addresses some of the limitations of on-board lamps. The diffuser is a calibrated reflectance standard that is illuminated by the Sun. Diffuser approaches can provide a full-aperture calibration using the entire optical path and the same illumination source as the desired scenes. One drawback is that now the calibrator may be located outside the satellite enclosure, and it is therefore more easily damaged by debris or exposure to excessive ultra-violet radiation. The calibrations can not be performed as often as those using a lamp because the proper geometry is generally only achieved at certain points during the orbit. For instance the MISR sensor deploys Spectralon® diffusers monthly over the North and South Poles (Bruegge et al., 1995).

The primary limitation of on-board calibrators is that after launch the calibration source can not be easily recalibrated, making it difficult to positively attribute changes to either the sensor response or the calibrator. For instance, the radiance from a solar diffuser could experience reflectance losses due to proton and ultraviolet irradiance (Slater and Palmer, 1991). This leads to the final type of calibration approaches, vicarious calibration, including several methods which all use a target external to the sensor. In a similar fashion to the solar diffuser that provides a calibration of the full optical path using the sun as a source. For a target to be of use in vicarious calibration, its radiance must be known or predicted when the sensor is viewing it. Therefore, it must be stable with respect to time or measurable at the time the sensor views it. The moon has been shown to have a stable radiance for a given phase angle and solar distance, and measurements are currently being

made to determine the absolute radiance values (Kieffer and Wildey, 1996). Once those values are known, a sensor platform could be rotated for a lunar view and a calibration coefficient can be determined.

In addition to the moon as a vicarious calibration source, the surface of the earth can be used. The Remote Sensing Group (RSG) of the University of Arizona's Optical Sciences Center has developed three methods of vicarious calibration of Earth-viewing sensors in the solar-reflective spectral range using the surface of the earth as the source. The reflectance-based approach involves measuring the surface reflectance of the target site and the atmospheric conditions over the site at the time of overpass. These data are used to derive inputs for a radiative transfer code (RTC) which calculates the top-of-atmosphere (TOA) radiance at the sensor. The RTC used is a modified version of the Gauss-Seidel iteration approach (Herman and Browning, 1965). The irradiance-based approach uses a measurement of the ratio of diffuse-to-global irradiance at ground level to further improve the characterization of the aerosols (Biggar et al., 1990a; Thome et al., 1997). The radiance-based approach relies on measurements of the up-welling radiance from the test site from a well-calibrated radiometer that is often mounted in an aircraft. Since the RTC is only used to model the atmosphere between the aircraft and the sensor the uncertainties due to atmospheric effects are reduced (Biggar, 1990b; Hovis et al., 1985). The radiance-based method has also been applied in the extreme case where the calibrated detector used is another satellite sensor viewing the same site at nearly the same time (Gustafson-Bold and Thome, 1996).

The reflectance- and irradiance-based methods require a measurement of the surface reflectance at the time of the sensor overflight. The measurements begin by pointing a spectroradiometer normal to a reference panel and measuring the upwelling radiance. Then the radiometer is adjusted to view the surface at the angle the sensor to be calibrated is viewing it, and the operator slowly walks the site measuring the upwelling radiance from the surface. The operator returns to measure the radiance from the reference several times during the data collection and after the site is completely measured. This allows for a more accurate correction of the effects of changing solar angles and drift of the spectroradiometer's response. The output from the spectroradiometer while viewing the reference is combined with the known bi-directional reflectance factor (BRF) of the reference and interpolated to calculate the BRF of the surface for the particular incident and view geometry at the time of the surface measurement. This value is then used as an input for the RTC.

The spectroradiometer used by the RSG has three detectors covering a spectral range from 350 - 2500 nm at a 1 nm interval. The collection optics include an optical fiber and a fore-optic which defines the field of view (FOV). A large FOV provides a spatial averaging of the surface so that small scale features are not disproportionately weighted, while a small FOV minimizes the effects of stray light reflected from the operator. The RSG uses the 8° FOV as a reasonable compromise between these two effects.

As mentioned previously, a reference panel with known BRF characteristics is needed to measure surface reflectance in the field. The reference used by the RSG measures 45 cm to a side and the BRF of the reference is measured in the laboratory versus a pressed polytetraflouroethylene (PTFE) sample. The BRF of the PTFE sample is determined from

6°/hemispheric reflectance factors (Biggar et al., 1988) supplied by the National Institute of Standards and Technology (NIST, then the National Bureau of Standards)(Weidner and Hsia, 1981). Although NIST dictates the use of a PTFE powder sold under the brand name of Halon® which is no longer available, the RSG uses Algoflon F6 that has been found to be a suitable replacement (Spyak and Lansard, 1997). A more detailed description of the BRF measurements is given in Appendix A.

Currently, the surface reflectance retrieval assumes that the illumination on the reference panel is due solely to the direct solar beam. In actuality, the illumination includes diffuse sky light as well as the solar beam. The errors introduced by neglecting this contribution is on the order of ±1% at a wavelength of 550 nm for a barium sulfate panel with good lambertian characteristics and normal atmospheric conditions (~20 km visibility) (Gu and Guyot, 1993). RTC runs show that the TOA radiance changes proportionally with the surface reflectance, which means that improvements to the calculation of the surface reflectance translate directly to improvements in the calibration of the sensor. The reflectance input for the RTC is supposed to be a bi-directional value, and so the primary purpose of the present dissertation is to develop a surface reflectance retrieval that eliminates the effect of the diffuse sky radiance.

The current work also includes several other changes that have been made to the calculation of the surface reflectance and the addition of a graphical user interface (GUI) to the processing software. A more thorough discussion of the theory of the current surface reflectance retrieval is presented in Chapter 2. Chapter 3 then discusses methods of deriving a bi-directional reflectance using RTC output, shaded reference measurements, and/or shaded

surface measurements. Chapter 4 presents the results of applying the diffuse corrections to reflectance data collected from calibrated reflectance tarpaulins and from the White Sands Missile Range test site in New Mexico. Chapter 5 discusses the inclusion of ancillary data to the reflectance calculation and the possibility of modeling the effect of cumulus clouds on the calculated surface reflectance.

# CHAPTER 2

# FIELD REFERENCE PANEL CALIBRATION

In order for the RTC to calculate the TOA radiance, the data required are the surface reflectance, the atmospheric optical thickness, $\delta$, and the aerosol size distribution or scattering phase function. If the BRF of the surface or the upwelling radiance at some level in the atmosphere is known, the RTC can be further constrained to obtain a more accurate answer.

The method used by the RSG for surface reflectance measurements in the field relies on having a calibrated reference panel. This chapter first describes the method the RSG uses to calibrate the reference panel in the laboratory. This calibration must be interpolated in both wavelength and angle for use in the field, and the methods used for these interpolations are presented in this chapter as well.

## Laboratory Calibration of Field Reference

The bi-directional reflectance factor (BRF) of a panel is the ratio of the radiance reflected into a given direction to the amount which a perfect lambertian diffuser would reflect into the same direction (Schott, 1997). It is defined as in Equation 2.1 where the

$$BRF_{\lambda}(\theta_v,\phi_v;\theta_i,\phi_i)=\pi BRDF_{\lambda}(\theta_v,\phi_v;\theta_i,\phi_i) \qquad 2.1$$

subscripts $v$ and $i$ indicate view and incident angles, $\pi$ is in steradian (sr) and BRDF is the bi-directional reflectance distribution function in $sr^{-1}$ and is given in Equation 2.2 where L

$$BRDF_{\lambda}(\theta_v,\phi_v;\theta_i,\phi_i)=\frac{L_{\lambda}(\theta_v,\phi_v)}{E_{\lambda}(\theta_i,\phi_i)} \qquad 2.2$$

is the upwelling radiance [W $m^{-2}$ $sr^{-1}$ $\mu m^{-1}$] and E the downwelling irradiance [W $m^{-2}$ $\mu m^{-1}$]. The BRF can be measured relatively using a ratio with a reflectance standard for which the BRF is already known. Reflectance standards have been successfully calibrated for BRF in the field using the sun as the illumination source (Jackson et al., 1987; Walter-Shea et al., 1993). While the use of the sun during the panel calibration eliminates some errors due to differences in the spectral shape of the sun versus a lamp, the field calibration procedure requires clear skies during the time of the measurement. Since laboratory measurements can be better controlled and can be performed on demand, the RSG performs calibrations of its field-reflectance panels in a specially-prepared laboratory. Since these laboratory measurements are critical to the reflectance retrievals for the RSG's vicarious methods, it is worthwhile to summarize the method as presented in Biggar et al. (1988).

A pressed polytetrafluoroethylene powder sample is prepared according to the procedure described by Weidner and Hsia (1981). Halon, the brand of PTFE powder used by Weidner and Hsia, has been discontinued so the RSG uses Algoflon F6 that has been found to be a suitable substitute for Halon. Therefore, the hemispherical reflectance factor with a 6° incident angle is assumed to be known for the pressed PTFE reference for wavelengths between 200 nm and 2500 nm.

The pressed PTFE is illuminated with a 1000 W DXW lamp powered by a current of 8 Amps at 120 V. A radiometer measures the radiance reflected normal to the pressed PTFE sample, while the angle of incidence is varied using computer controlled rotation stages. The lower limit of measured incidence angles is determined by the angle at which the radiometer begins to shadow the panel and the smallest angle possible is currently 15° for measurements in the VNIR. To reduce the effects of reflected radiance from outside the radiometers nominal field of view, a Barium Sulfate panel with a hole cut in the center is placed around the Algoflon sample during measurements to better duplicate the conditions

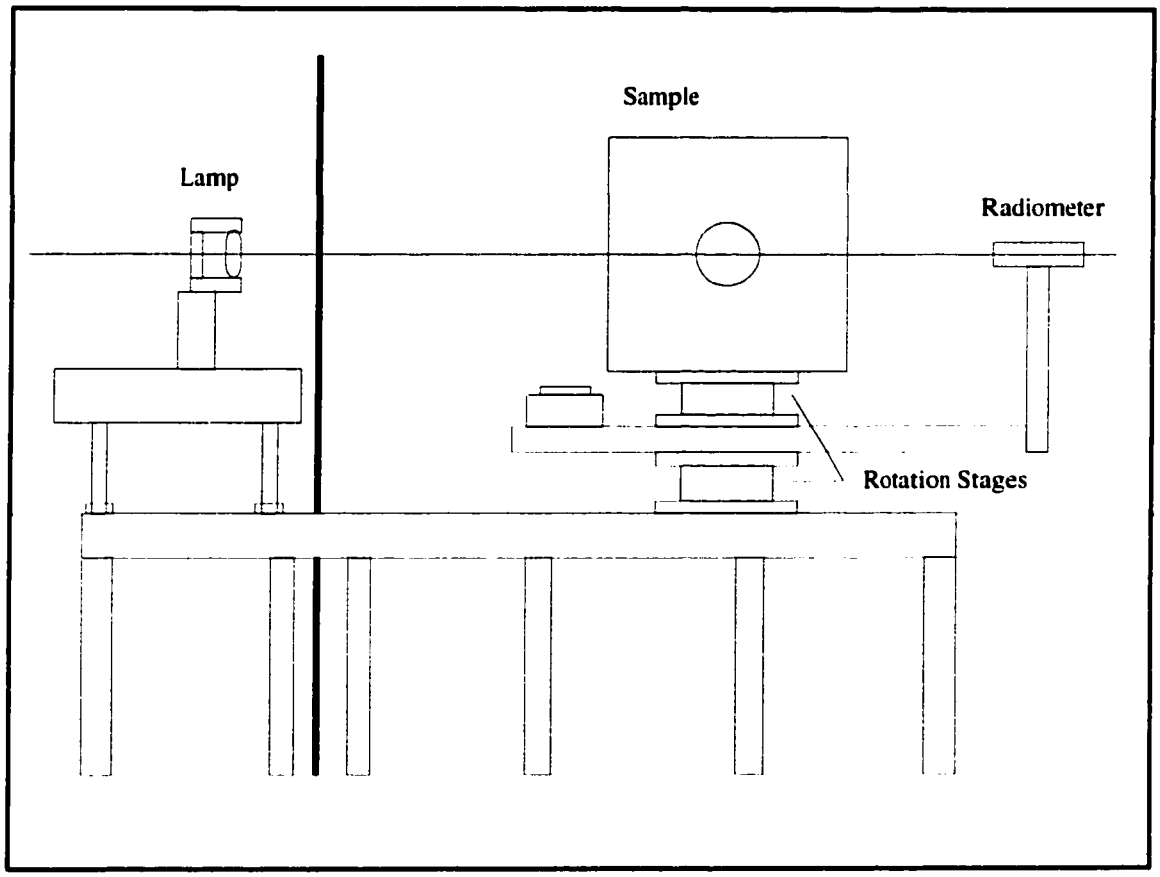


**Figure 2.1** Black lab set up for BRF measurements.

when the large field reference panels are measured. Figure 2.1 is an illustration of the laboratory set-up. The optical axis is defined using a Helium-Neon laser, and the lamp, sample and radiometer are all centered on the optical axis. Stray reflections from around the room can influence the measurements so all the exposed surfaces in the laboratory are blackened, including the floors, ceiling, walls, doorknobs, table tops, etc. To further reduce stray reflections, the lamp is located in an adjoining room and illuminates the samples through a 5 cm aperture in the wall.

The method which the RSG uses to measure the BRF of the field reference panels is described in detail in Appendix A. The values returned are the BRF's of the field reference for the 21 wavelengths listed in Table 2.1 and incident angles from 10° - 75° at 5° steps. As was mentioned in Chapter 1, the spectroradiometer used in the field returns values every 1 nm from 350 nm - 2500 nm, so it is necessary to interpolate spectrally in order to apply the laboratory measurements to the field data. Similarly the laboratory values must be interpolated in angle to account for the particular solar angle at the time of the field data collection.

| Silicon | Indium Antimonide |
|---|---|
| 401 | 747 |
| 455 | 869 |
| 502 | 940 |
| 553 | 1243 |
| 650 | 1646 |
| 699 | 2134 |
| 800 | 2164 |
| 845 | 2207 |
| 948 | 2262 |
| 1060 | 2332 |
| | 2403 |

**Table 2.1** Laboratory radiometer wavelengths in nanometers.

**Spectral Interpolation**

The spectroradiometer used for surface reflectance measurements outputs data from 350 - 2500 nm at 1-nm increments. It is therefore necessary to interpolate the data from the black lab measurements to these wavelengths. Previously, this was accomplished by using a least squares polynomial fit to the spectral data at each measured incidence angle. Figure 2.2 plots the difference between a 4$^{th}$ and 6$^{th}$ order polynomial fitted to the same discrete laboratory data. The differences of 1% in the interpolated values and 2% in the extrapolated

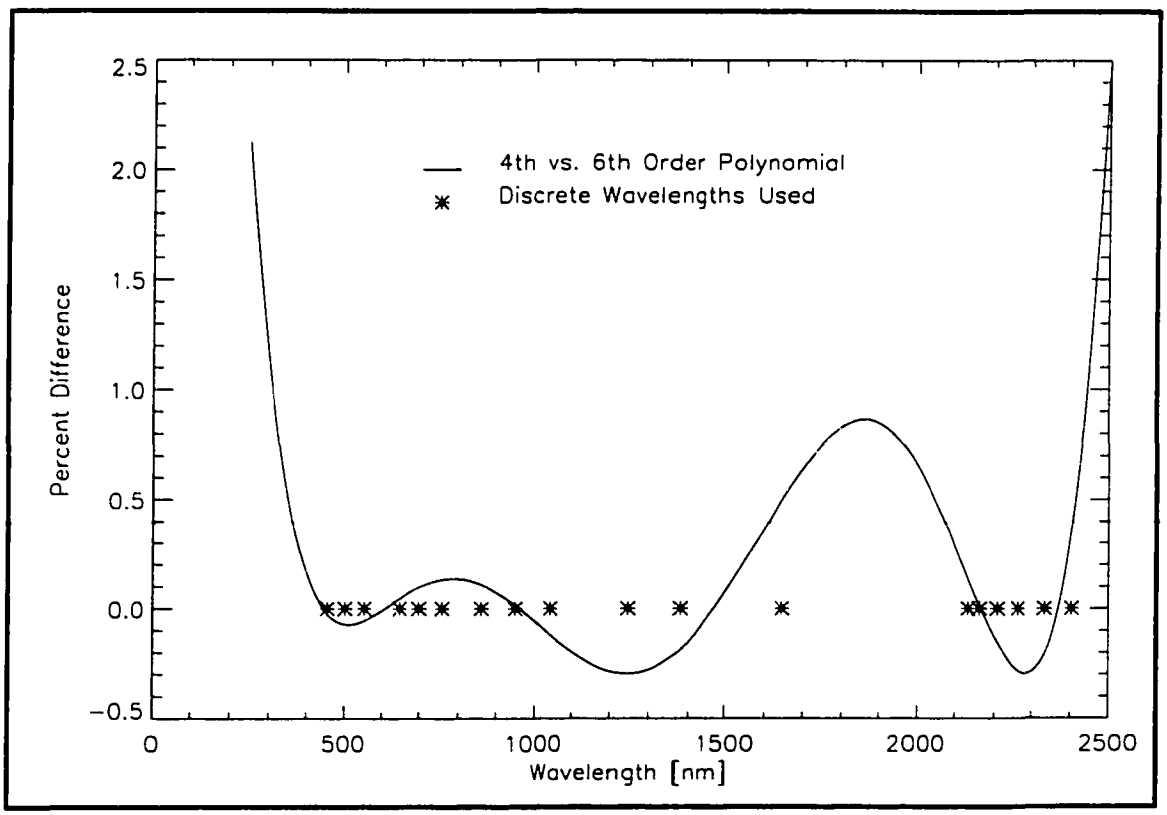


**Figure 2.2** Percent difference between the BRF of a reference panel as interpolated using 4$^{th}$ and 6$^{th}$ order polynomial fit to discrete laboratory data.

values are of the same order of magnitude as the effect of the diffuse radiance, so a more correct interpolation must be used.

Since there is no scientific reason to claim that one order polynomial is more accurate than another, an interpolation scheme with a physical basis was developed and this requires spectral measurement of the field reference at high spectral resolution. An attempt was made to measure the hemispherical reflectance of a piece of the reference panel material, but the resulting values had obvious errors, such as hemispherical reflectances greater than 1, which made them unusable. This dissertation will use hemispherical reflectance data supplied by the manufacturer at 1 nm intervals from 350 to 2500 nm (Labsphere, 2000). These data are plotted in Figure 2.3 along with the hemispherical reflectance of pressed PTFE powder as reported by Weidner and Hsia of NBS, now NIST (Weidner and Hsia, 1981).

The hemispherical reflectance data were shifted and tilted to achieve a best fit in an unweighted least squares sense to the discrete BRF data. The interpolated reflectance is given by:

$$\rho_{interpolated}(\lambda) = (b + m\lambda)\rho_{hemispheric}(\lambda) \qquad 2.3$$

where m and b are given by Equations 2.4 and 2.5.

$$m = \frac{\sum BRF_i \rho_{hemi_i} - b \sum \rho_{hemi_i}^2}{\sum \rho_{hemi_i}^2 \lambda_i} \qquad 2.4$$

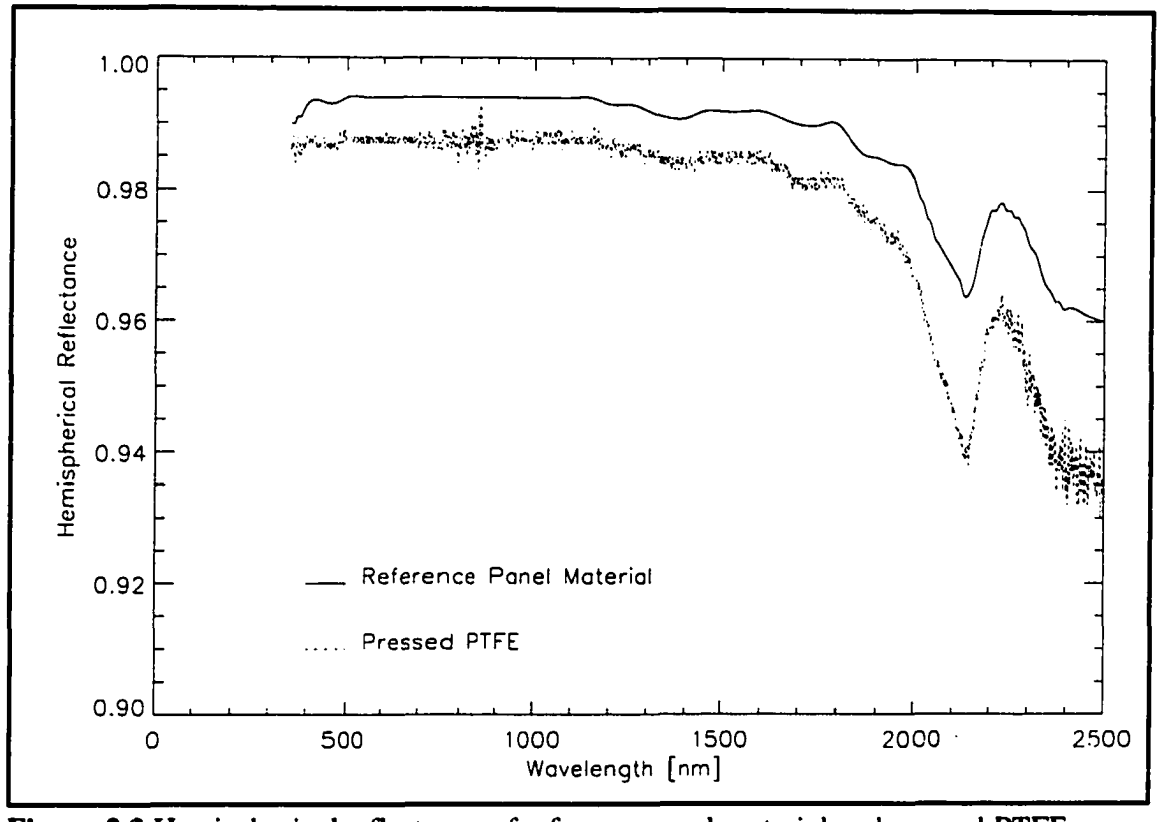


**Figure 2.3** Hemispherical reflectance of reference panel material and pressed PTFE powder.

$$b = \frac{\sum BRF_i \rho_{hemi_i} \lambda_i - \frac{\sum \rho_{hemi_i}{}^2 \lambda^2{}_i \sum BRF_i \rho_{hemi_i}}{\sum \rho_{hemi_i}{}^2 \lambda_i}}{\sum \rho_{hemi_i}{}^2 \lambda_i - \frac{\sum \rho_{hemi_i}{}^2 \sum \rho_{hemi_i}{}^2 \lambda_i^2}{\sum \rho_{hemi_i}{}^2 \lambda_i}} \qquad 2.5$$

Where $BRF_i$ is the discrete BRF measured in the laboratory, $\lambda_i$ is the wavelength which corresponds to $BRF_i$, and $\rho_{hemi\,i}$ is the hemispherical reflectance at $\lambda_i$. Some of the SWIR filters are located on the edges of the absorption feature so in order to ensure an accurate fit, the filter transmittances from the laboratory radiometer were used to determine a band-averaged value for $\rho_{hemi\,i}$ at those wavelengths. Equations 2.4 and 2.5 are derived by performing a least squares fit of Equation 2.3 to the discrete directional reflectance data from the blacklab. Using these equations is equivalent to shifting and tilting the hemispheric data to best fit the discrete directional data. Figure 2.4 shows the discrete BRF values, a $4^{th}$ order polynomial interpolation of those data, and the scaled hemispheric values. Figure 2.5 plots the percent difference between the discrete values and the interpolation data evaluated at the original discrete wavelengths. The agreement of the hemispherical reflectance interpolation is comparable to the polynomial at the short wavelengths, and is a much better fit to the absorption feature in the SWIR. The improved fit in the SWIR combined with the physical basis for this interpolation method are the reasons it was selected.

**Angular Interpolation**

When measuring the reference panel in the field the radiometer is positioned normal to the panel and the incident angle is the solar zenith angle. Since the measured values for the panel BRF are at 5° increments it is necessary to angularly interpolate in order to accurately describe the panel BRF at the time of the measurement. These data are fit using a least squares polynomial where the coefficient of the linear term is constrained to be zero forcing the derivative of the interpolated data to equal zero for a 0° incidence angle. The reference panel material has a negligible specular peak, and this constraint models that

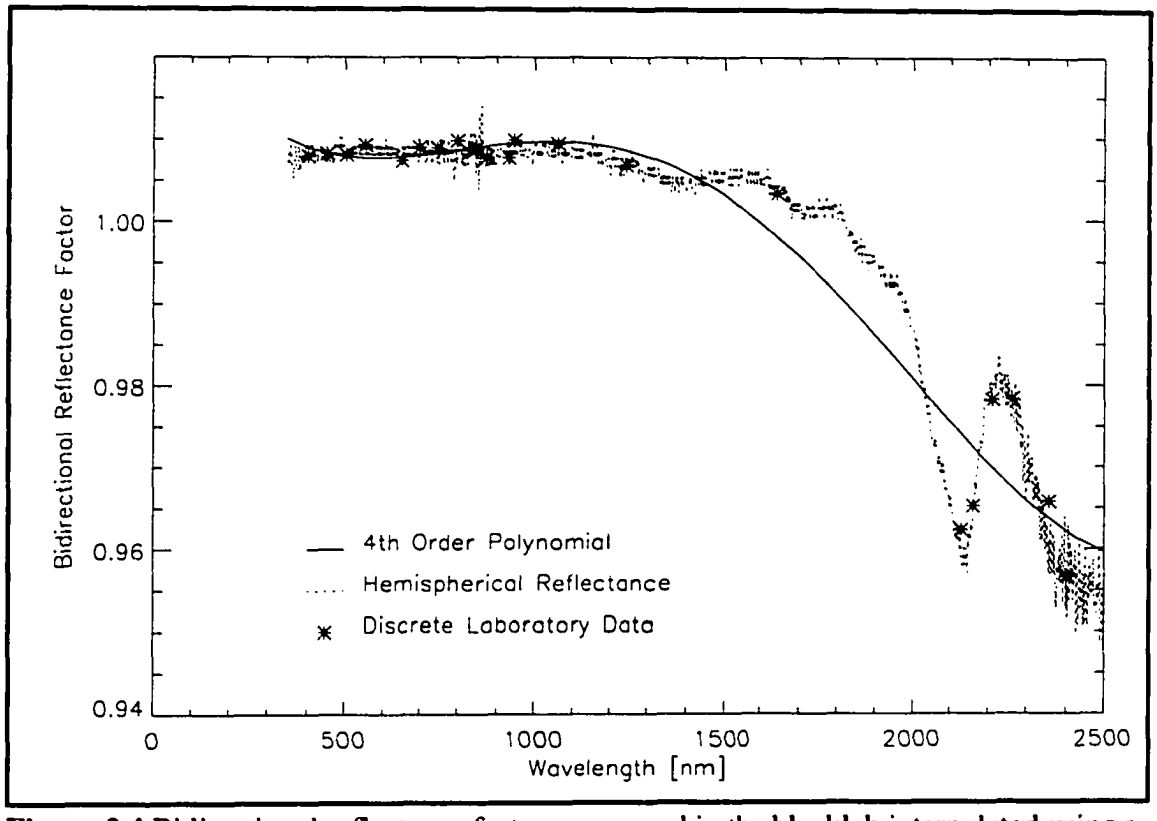


**Figure 2.4** Bidirectional reflectance factors measured in the blacklab interpolated using a 4th order polynomial and a linear scaling of the hemispherical reflectance.

behavior in the absence of data collected for 0° incidence where the radiometer is shadowing the reference panel.

A 4th and a 6th order polynomial with the above constraint was fit to 554 nm laboratory data from 17 May 1999. Figure 2.6 plots the percent difference between the interpolated values as calculated using the 4th and 6th order fits. Unlike the wavelength interpolation, the order of the polynomial does not significantly change the interpolated values. In Figure 2.7 the difference between the laboratory data and the 4th order fit evaluated at the laboratory angles is plotted along with error bars which represent the uncertainty in the laboratory measurements. The fitted data agrees with discrete values to

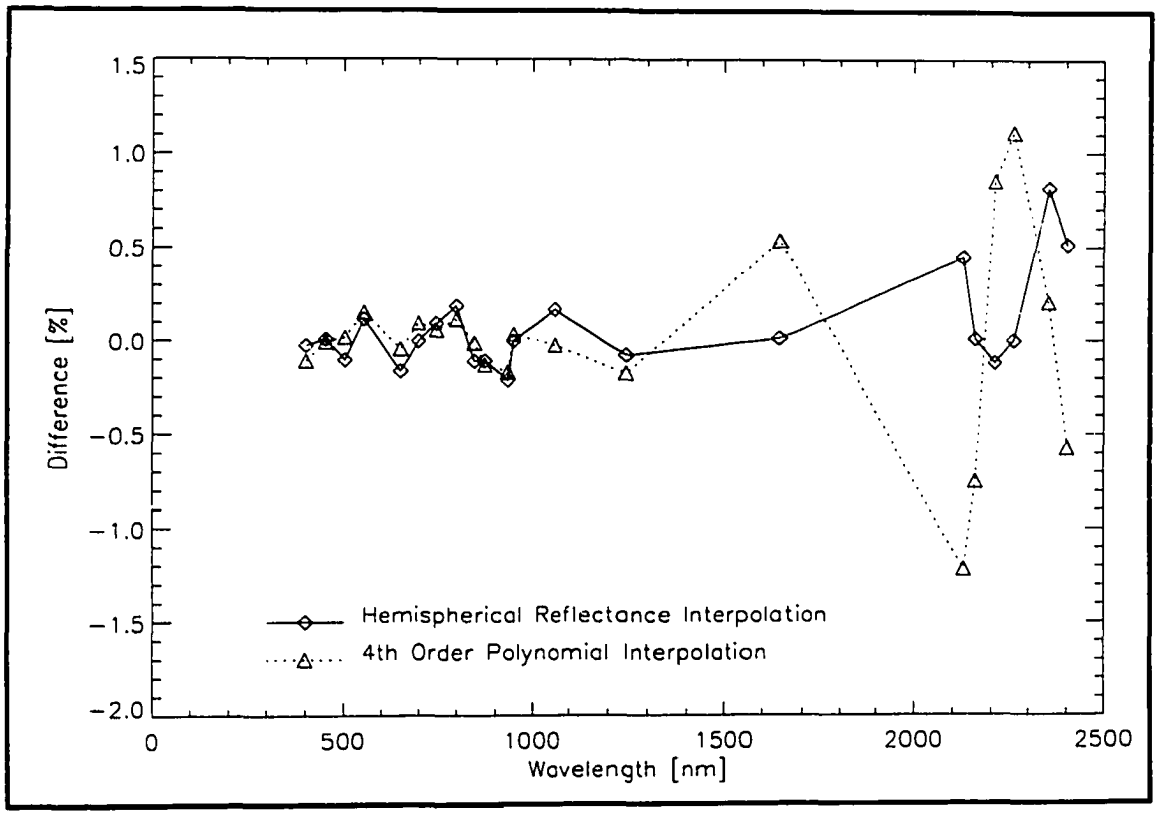


**Figure 2.5** Percent difference between discrete BRF data and interpolations evaluated at the discrete wavelengths.

within the uncertainty of the measurements at all angles. Because of the polynomials favorable agreement with the laboratory data and its weak dependence on polynomial order, the angular interpolation is performed using a $4^{th}$ order polynomial.

The wavelengths needed for the field data are known and constant for a particular instrument, while the incident angles needed are the solar zenith angles at the time of each measurement. For this reason the spectral interpolation is performed first, then the angular. The coefficients of the angular fits for each wavelength are saved to an ASCII file for easy use on either a Intel or Sun based system.

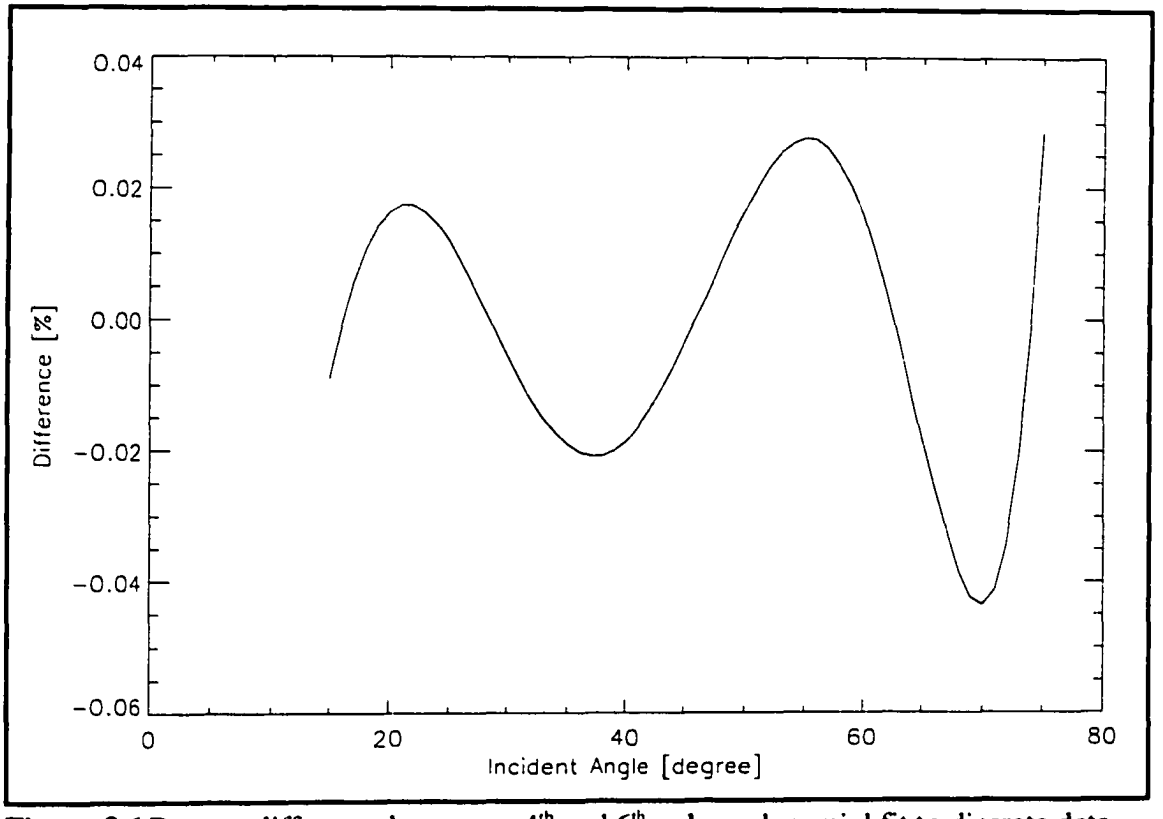


**Figure 2.6** Percent difference between a 4th and 6th order polynomial fit to discrete data from 17 May 1999 @ 554 nm.

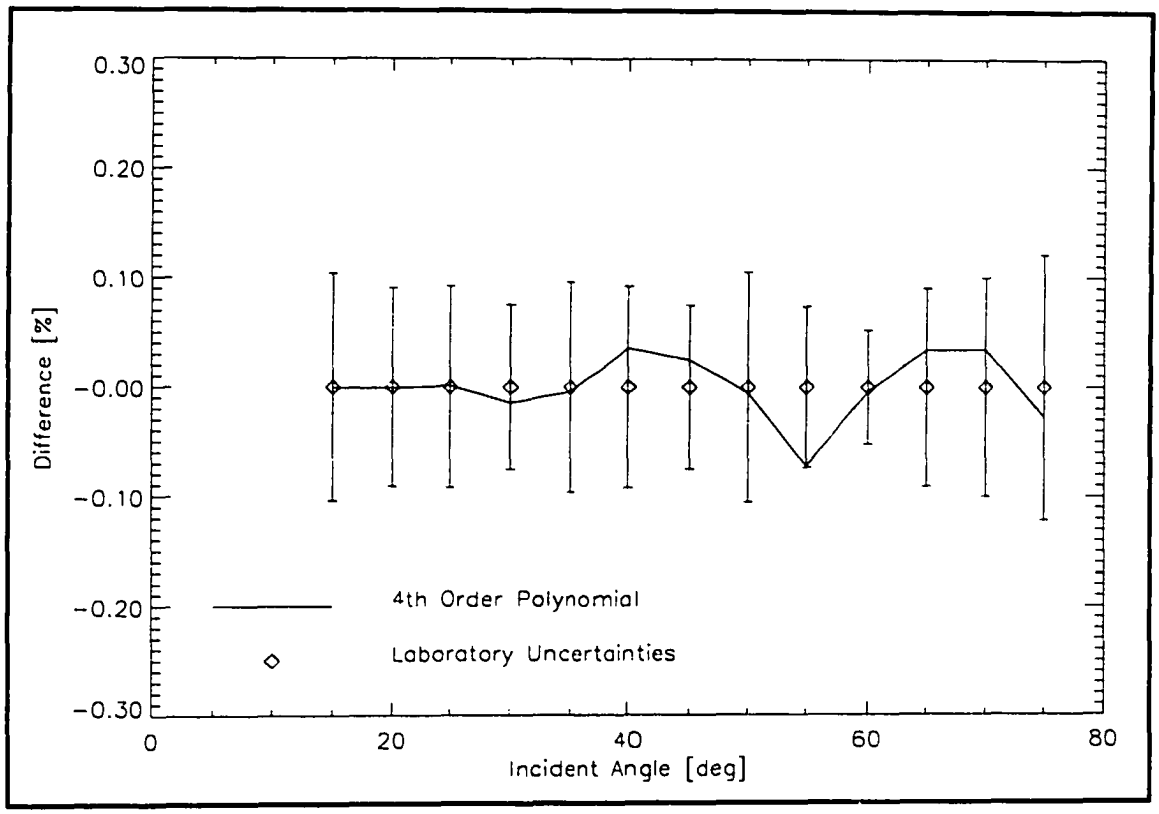


**Figure 2.7** Percent difference between interpolated BRF and discrete values.

# CHAPTER 3

# DIFFUSE CORRECTION METHODS

The RTC used by the RSG to calculate the top-of-atmosphere (TOA) radiance seen by the sensor requires a nadir-view surface reflectance as one of its inputs. When measuring the upwelling radiance from the reference panel or the surface in the field, the signal is dominated by the reflected radiance of the directly-transmitted solar irradiance. The other source of reflected radiance is that due to downwelling sky irradiance. Although the effect of this diffuse light is typically small for the RSG's test sites, it has been shown that errors in the surface reflectance propagate through as equal errors in the TOA radiance (Biggar, 1990b) thus, the small effect due to diffuse light can still be significant.

This chapter discusses the effect of the diffuse radiance as determined using modeled data from the RTC. Three methods for removing diffuse-light effects in the surface reflectance retrieval are presented based on various combinations of field data and RTC runs. Also included is an examination of the sensitivity of these diffuse corrections to the various input parameters.

**Effect of Diffuse Radiance on Field BRF Retrieval**

To determine the reflectance of a surface, the upwelling radiance from the surface is compared to the upwelling radiance from a reference panel with known reflectance properties. In the field, there are two sources of incident irradiance which must be considered: the directly-transmitted solar beam and the downwelling diffuse sky irradiance. The reflected radiance due to directly-transmitted solar irradiance, $L_{sol}$, and the reflected radiance due to diffuse sky irradiance, $L_{diff}$, can be written as

$$L_{sol}(\theta_{view},\phi_{view}) = E_{sol}\cos\theta_{sol}e^{-\tau(\theta_{sol})}\frac{BRF(\theta_{sol},\phi_{sol};\theta_{view}\phi_{view})}{\pi} \quad 3.1$$

$$L_{diff}(\theta_{view},\phi_{view}) = \int_0^{2\pi}\int_0^{\frac{\pi}{2}} L_{sky}(\theta_{inc},\phi_{inc})\frac{BRF(\theta_{inc},\phi_{inc};\theta_{view},\phi_{view})}{\pi}\cos\theta_{inc}\sin\theta_{inc}d\theta_{inc}d\phi_{inc} \quad 3.2$$

where $E_{sol}$ is the exoatmospheric solar irradiance, $L_{sky}(\theta_{inc},\phi_{inc})$ is the at-surface diffuse radiance, $\theta$ and $\phi$ are the zenith and azimuth for the incident, view, and solar angles, and $\tau(\theta_{sol})$ is the atmospheric slant-path transmittance for the angle $\theta_{sol}$. Throughout this chapter the values used are spectral, but the $\lambda$ subscript is omitted to simplify the notation.

One input required by the radiative transfer code (RTC) used by the RSG is the bi-directional reflectance of the site for the given solar zenith angle, $\theta_{sol}$, and a nadir view such that, $\theta_{view} = 0$. Figure 3.1 illustrates the angular convention. Using the known BRF of the reference panel, the bi-directional reflectance of the site, $\rho_{surf}$, is given by

$$\rho_{surf} = \rho_{panel}\frac{L_{sol}}{L'_{sol}} \quad 3.3$$

where $L_{sol}$ and $L'_{sol}$ are the reflected radiance from the surface and from the reference panel due to the direct solar irradiance and $\rho$ is used in place of $BRF(\theta_{sol},\phi_{sol};0,0)$ for both the surface and the reference panel in order to simplify the notation. Throughout this work,

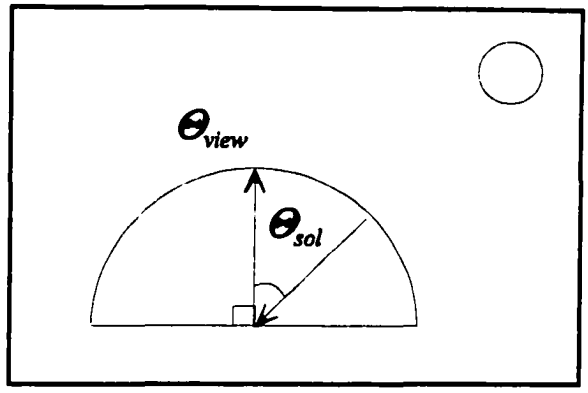


**Figure 3.1** Solar and view zenith angle convention.

primed quantities indicate that the value is related to the reference panel, and unprimed quantities refer to the surface.

Measuring $L_{sol}$ or $L'_{sol}$ requires that the only incident irradiance be from the directly-transmitted solar beam. Diffuse radiance in the field comes from all directions, so limiting the incident radiance to the solar beam would require something akin to a opaque dome with an aperture which can move in $\theta$ and $\phi$ to admit the solar beam and an aperture to measure the radiance. This is physically impractical, thus, the radiance that is measured is a sum of both direct and diffuse terms,

$$L_{total} = L_{sol} + L_{diff}$$
$$L'_{total} = L'_{sol} + L'_{diff} \qquad 3.4$$

where $L_{total}$ is the reflected radiance due to the total downwelling irradiance incident on the surface and $L'_{total}$ is the reflected radiance due to the total downwelling irradiance incident on the reference panel.

Using $L_{total}$ and $L'_{total}$ a value for $\rho_{surf}$ can be calculated as:

$$\rho_{surf} = \rho_{panel} \frac{L_{total}}{L'_{total}} \qquad 3.5$$

where $L_{total}$ and $L'_{total}$ have been used instead of $L_{sol}$ and $L'_{sol}$ respectively in Equation 3.3. This calculation of $\rho_{surf}$ differs from Equation 3.3 with wavelength depending on the relative contributions of the diffuse sky irradiance to the illumination of the surface and reference. For cases where the scattering optical depth is small, e.g. long wavelengths, the contribution of the diffuse sky irradiance can be neglected. However in the presence of strong scattering this effect can lead to appreciable differences between the reflectances retrieved using 3.3 and 3.5.

The expression for $\rho_{surf}$ can be rewritten as

$$\rho_{surf} = \rho_{panel} \frac{\{E_{sol}\cos\theta_{sol}e^{-\tau(\theta_{sol})}\frac{BRF_{surf}(\theta_{sol},\phi_{sol};0,0)}{\pi} + \int_0^{2\pi}\int_0^{\frac{\pi}{2}}\frac{BRF_{surf}(\theta_{inc},\phi_{inc};0,0)}{\pi}L_{sky}(\theta_{inc},\phi_{inc})\cos\theta_{inc}\sin\theta_{inc}d\theta_{inc}d\phi_{inc}\}}{\{E_{sol}\cos\theta_{sol}e^{-\tau(\theta_{sol})}\frac{BRF_{panel}(\theta_{sol},\phi_{sol};0,0)}{\pi} + \int_0^{2\pi}\int_0^{\frac{\pi}{2}}\frac{BRF_{panel}(\theta_{inc},\phi_{inc};0,0)}{\pi}L_{sky}(\theta_{inc},\phi_{inc})\cos\theta_{inc}\sin\theta_{inc}d\theta_{inc}d\phi_{inc}\}} \quad 3.6$$

combining Equations 3.1, 3.2, 3.4, and 3.5. When the surface and the reference panel are lambertian, $BRF_{surf}(\theta_{inc},\phi_{inc};0,0)$ and $BRF_{panel}(\theta_{inc},\phi_{inc};0,0)$ are constants. Equation 3.6 can be rewritten as

$$\rho_{surf} = \rho_{panel}\frac{BRF_{surf}}{BRF_{panel}} = \rho_{panel}\frac{L_{sol}}{L'_{sol}} \quad 3.7$$

when the constants are taken outside the integrals and identical terms are canceled. If both the reference panel and the surface are lambertian, the retrieved surface reflectance is the same whether or not the diffuse radiance is considered. Similarly, it can be shown that for any case where the surface BRF differs from the reference BRF by only a multiplicative constant, the hemispherical-direct and the direct-direct reflectance factors will be equal. When the non-lambertian properties of the surface and the reference are different the ratio of the reflected solar irradiances will not equal the ratio of the reflected total irradiances, and calculated surface reflectances will differ.

In order to determine the effect these non-lambertian properties have, several simulated data sets were produced, using a gauss-seidel RTC developed at the University of Arizona (Herman and Browning, 1965). The $L_{total}$, $L_{sol}$, and $L_{diff}$ reflected radiances were calculated for a spectrally flat reference with angular reflectance properties based on those of the RSG's site panel and for several simulated surface BRFs. The spectral dependance of the reference panel and surface BRFs were neglected so that the effects of the diffuse radiance could be more easily observed. Table 3.1 shows the inputs used for the RTC runs based on values from White Sands Missile Range on 29 October 1999.

The RTC was modified such that the output included the radiance field at the surface for each wavelength. Once the at-surface radiance field is obtained it is possible to calculate the reflected radiances described earlier using Equations 3.1, 3.2 and 3.4.

The RTC calculates radiances normalized to the exoatmospheric solar irradiance, meaning that the input energy is taken to be the cosine of $\theta_{sol}$. Now, the values for the pertinent radiances can be computed numerically using the RTC output.

Figure 3.2 shows the percent difference between the values of $\rho_{surf}$ calculated using Equations 3.3 and 3.5 using the lambertian surface and a spectrally-flat reference panel with non-lambertian BRF based on laboratory measurements of the RSG's reference panel. The cases shown are for the atmospheric assumptions of molecular scattering only and molecular and aerosol scattering with gaseous absorption by ozone with a number density of 0.256 $cm^{-3}$. In the pure molecular case, the scattering optical depth as a function of wavelength follows a $\lambda^{-4}$ dependence. As such, the errors at the longer wavelengths are small because there is not much energy in the diffuse field. At shorter wavelengths, the diffuse irradiance is larger and the error increases until approximately 400 nm, at which point the error begins to decrease again. This decrease in the error is caused by an interaction of the diffuse radiance field distribution, the solar zenith angle and the BRF of the reference panel.

| Parameter | Value |
|---|---|
| Junge Parameter | 3.7346 |
| Aerosol Index of Refraction | $1.44 + 0.005i$ |
| Aerosol Radius Range [μm] | [0.01, 5.01] @ 0.01 |
| View Angles ($\theta_{view}$,$\phi_{view}$) [degrees] | (00.0, 000.0) |
| Solar Angles ($\theta_{sol}$,$\phi_{sol}$) [degrees] | (52.5, 156.6) |
| Altitude Range [km] | [1.197, 50.0] |
| Pressure [mbars] | 809.42 |
| Ozone Number Density [$cm^{-3}$] | 0.256 |
| Aerosol Optical Depth @ 0.55 μm | 0.0517 |
| Lambertian $BRF_{surf}$ | 0.5 |

**Table 3.1** Input parameters for the RTC used to produce simulated data.

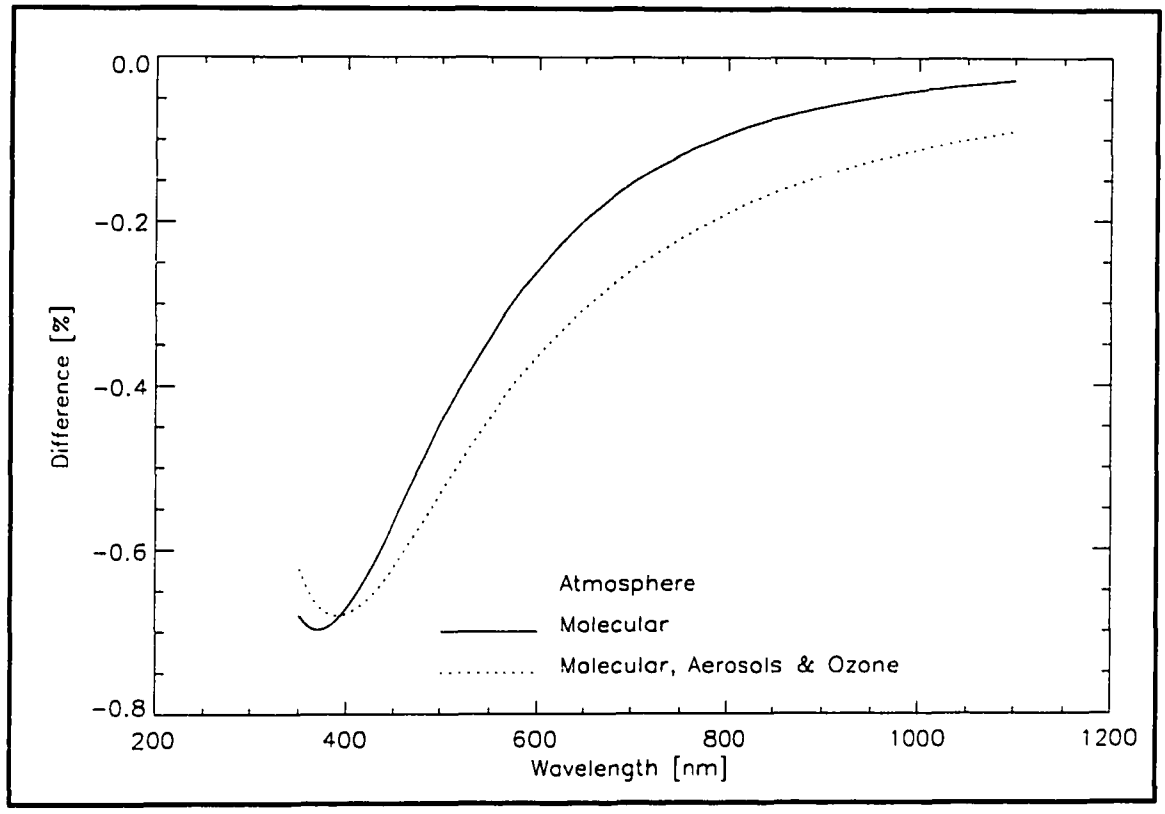


**Figure 3.2** Percent difference between directional-directional and hemispherical-directional surface reflectance.

In order to understand this interaction it is necessary to take a more in depth look at the effect of $L_{diff}$ and $L'_{diff}$ on $\rho_{surf}$. Equation 3.5 can be rewritten as

$$\rho_{surf} = \rho_{panel} \frac{L_{sol} + L_{diff}}{L'_{sol} + L'_{diff}} \quad . \qquad 3.8$$

Since the surface assumed is lambertian, there would be no differences between the reflectances calculated from Equations 3.3 and 3.5 if the reference were also lambertian, so a non-lambertian $BRF_{panel}$ is used. Figure 3.3 is a typical plot of the $BRF_{panel}$ as a function of incident angle and a nadir view for the RSG site panel. The BRF generally decreases with increasing incident zenith angle, so according to Equation 3.1 radiances incident at angles greater than $\theta_{sol}$ will be weighted less heavily than in the lambertian case. Similarly radiances incident at angles less than $\theta_{sol}$ will be more heavily weighted. Whether $L'_{diff}$ will be greater or less than the lambertian reference case depends on both the solar zenith angle

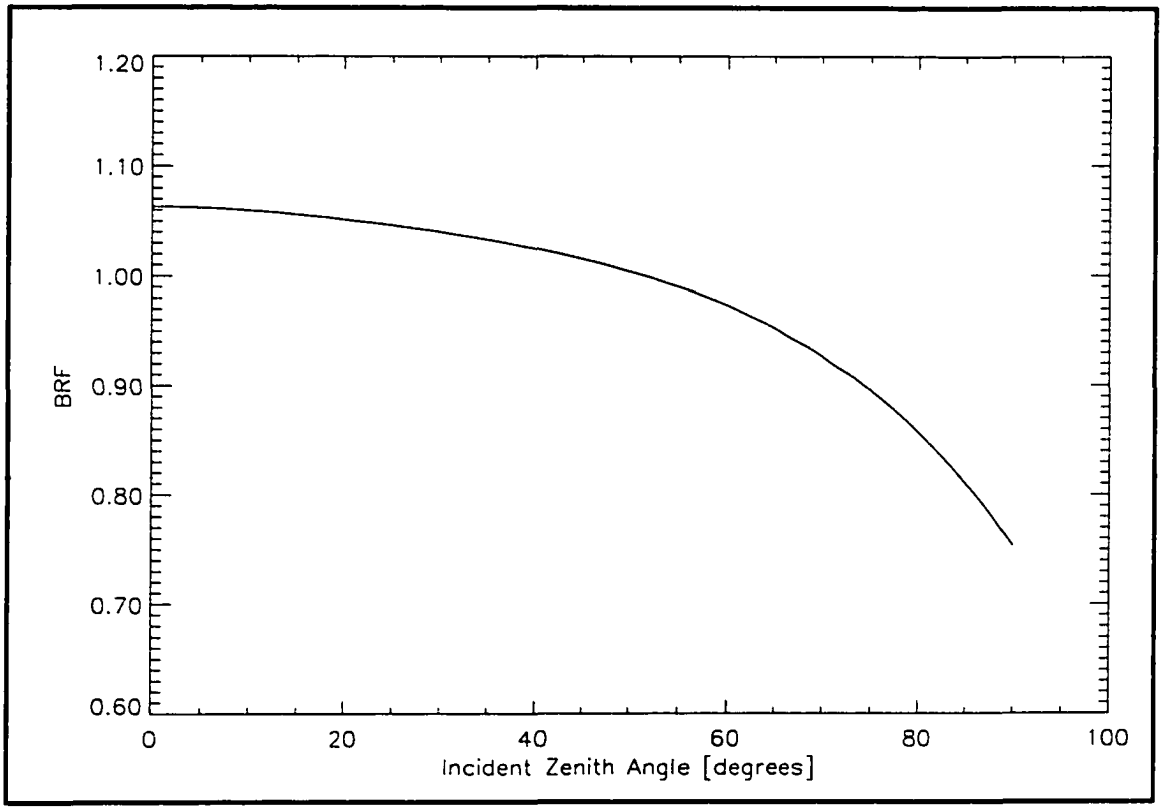


**Figure 3.3** BRF for a nadir view of the site panel measured at 500 nm.

and the distribution of $L_{sky}$. If $L'_{diff}$ is less than it would be for a lambertian reference, the denominator of Equation 3.8 is smaller, making the value of $\rho_{surf}$ greater. Similarly when $L'_{diff}$ is greater than in the lambertian case, $\rho_{surf}$ is less.

The dependence on the solar zenith angle is demonstrated by the cases of $\theta_{sol} = 0°$ and 76°. When $\theta_{sol} = 0°$ all of the diffuse radiances are from angles greater than $\theta_{sol}$. $L'_{diff}$ will therefore be less than it would be in the lambertian case, which makes the denominator in Equation 3.8 smaller leading to a larger $\rho_{surf}$. When $\theta_{sol} = 76°$ the diffuse radiances are primarily from angles less than $\theta_{sol}$ and $L'_{diff}$ is greater than the lambertian case, making $\rho_{surf}$ less than the true directional-directional value. This behavior can be seen in Figure 3.4, which is a plot of the percent difference in $\rho_{surf}$ as calculated using Equation 3.3 and 3.5 for solar zenith angles of 0°, 52° and 76°.

For $\theta_{sol} = 52°$ at long wavelengths, the behavior of the errors are similar to the 0° case, but at shorter wavelengths the magnitude of the percent difference stops increasing and begins decreasing. The RTC used assumes a flat plane-parallel atmosphere, which implies that the path length through the atmosphere approaches $\infty$ as $\theta$ approaches 90°. This extremely long path length allows for a much greater scattering as well as more attenuation from that direction, and so the magnitude of the radiance from near 90° is larger than that at 0°. In the case of a pure molecular atmosphere, as the optical depth increases (decreasing wavelength) the downwelling irradiance becomes more uniform and the ratio of the radiance from a zenith angle of 5° to the radiance from an 85° zenith angle increases as shown in Figure 3.5.

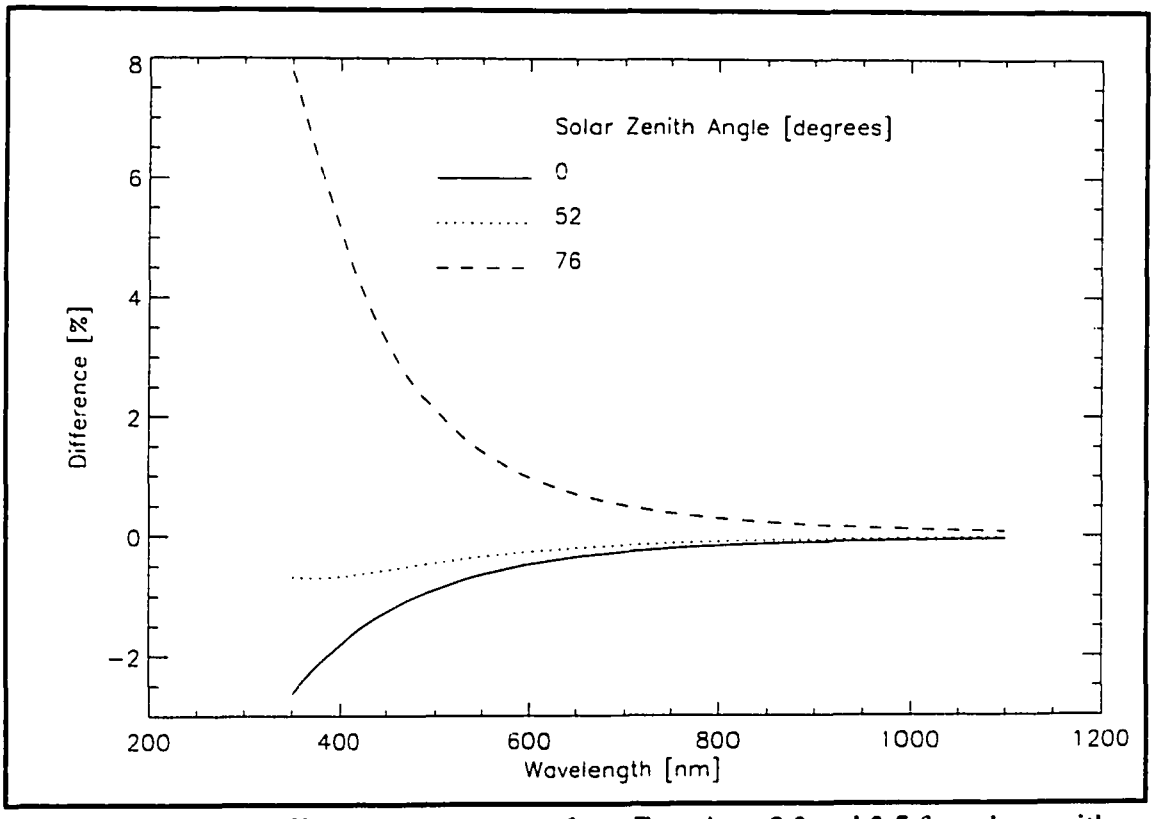


**Figure 3.4** Percent difference between $\rho_{surf}$ from Equations 3.3 and 3.5 for solar zenith angles of 0°, 52°, and 76°.

The addition of aerosols influence the distribution of radiance in two distinct ways, both of which cause the L(5°)/L(85°) ratio to increase at longer wavelengths as compared to the pure molecular atmosphere. The first contribution is the additional component to the total optical depth, which can be thought of as simply shifting the plots in Figure 3.5 to longer wavelengths. Second, the aerosols introduce absorption, thus the longer path lengths near the horizon lose more energy to absorption than paths near nadir, causing the L(5°)/L(85°) ratio to increase, as well. Including weak gaseous absorption in the

calculations has a similar effect as the addition of aerosols, except that the absorption is now stronger and spectrally dependent.

While the assumption of a lambertian surface makes it easier to understand the modeled data, the actual surfaces have non-lambertian properties contributing to changes in the calculated $\rho_{surf}$ as well. Figure 3.6 shows several forms of $BRF_{surf}$ which were examined. All of the surface BRFs follow the relationship

$$\frac{C}{\pi}\int_0^{2\pi}\int_0^{\frac{\pi}{2}} BRF_{surf}(\theta_{inc},\phi_{inc};0,0)\cos\theta_{inc}\sin\theta_{inc}d\theta_{inc}d\phi_{inc} = 0.5 \qquad 3.9$$

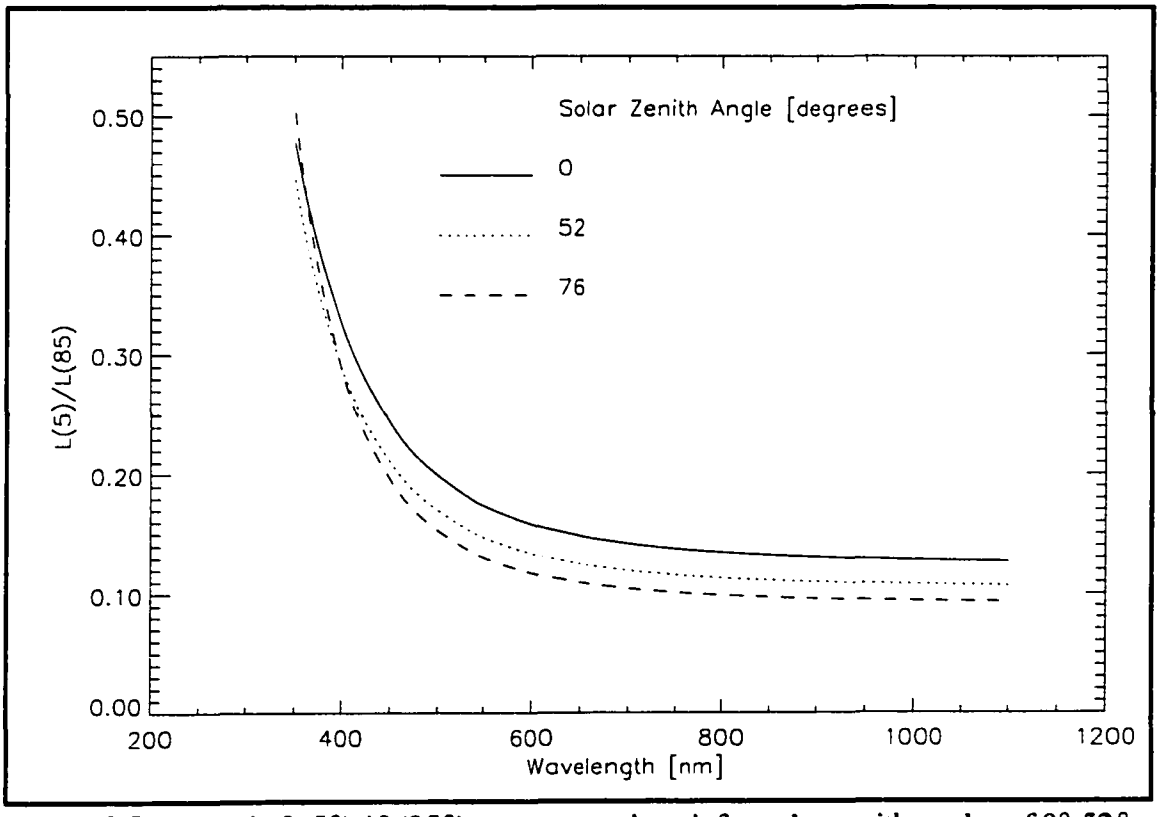


**Figure 3.5** The ratio L(5°) / L(85°) versus wavelength for solar zenith angles of 0°,52°, and 76°.

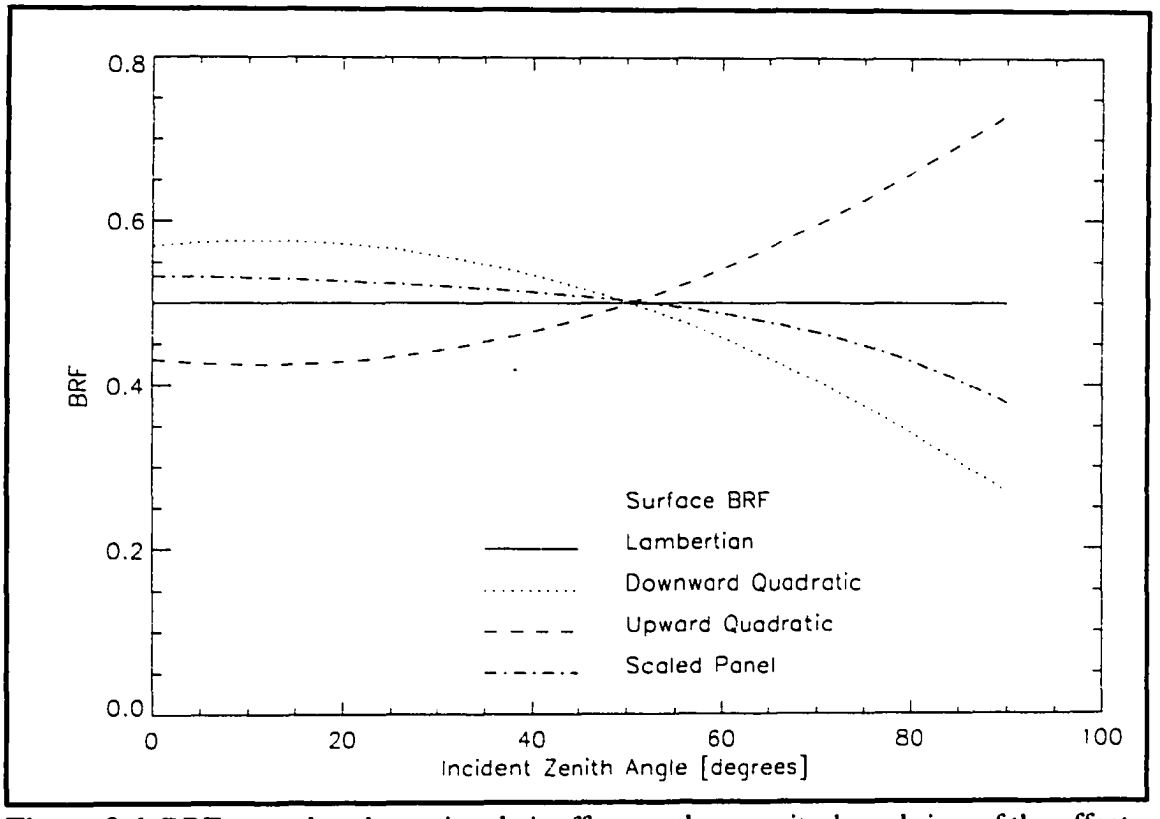


**Figure 3.6** $BRF_{surf}$ used to determine their effect on the magnitude and sign of the effect due to diffuse radiance.

where the constant C is a scale factor to ensure that the total energy reflected from the surface is the same in all cases. Figure 3.7 shows the percent effect of using Equation 3.5 instead of 3.3 to calculate $\rho_{surf}$ for each $BRF_{surf}$ plotted in Figure 3.6. As was stated before, any case where the shape of the $BRF_{surf}$ matches that of the reference panel, that is $BRF_{surf} = A * BRF_{panel}$, with A being a constant, the difference is zero. In the case where $BRF_{surf}$ varies in the opposite sense as $BRF_{panel}$ the contributions of the two BRF's are cumulative and the total effect is greater than that for the lambertian surface.

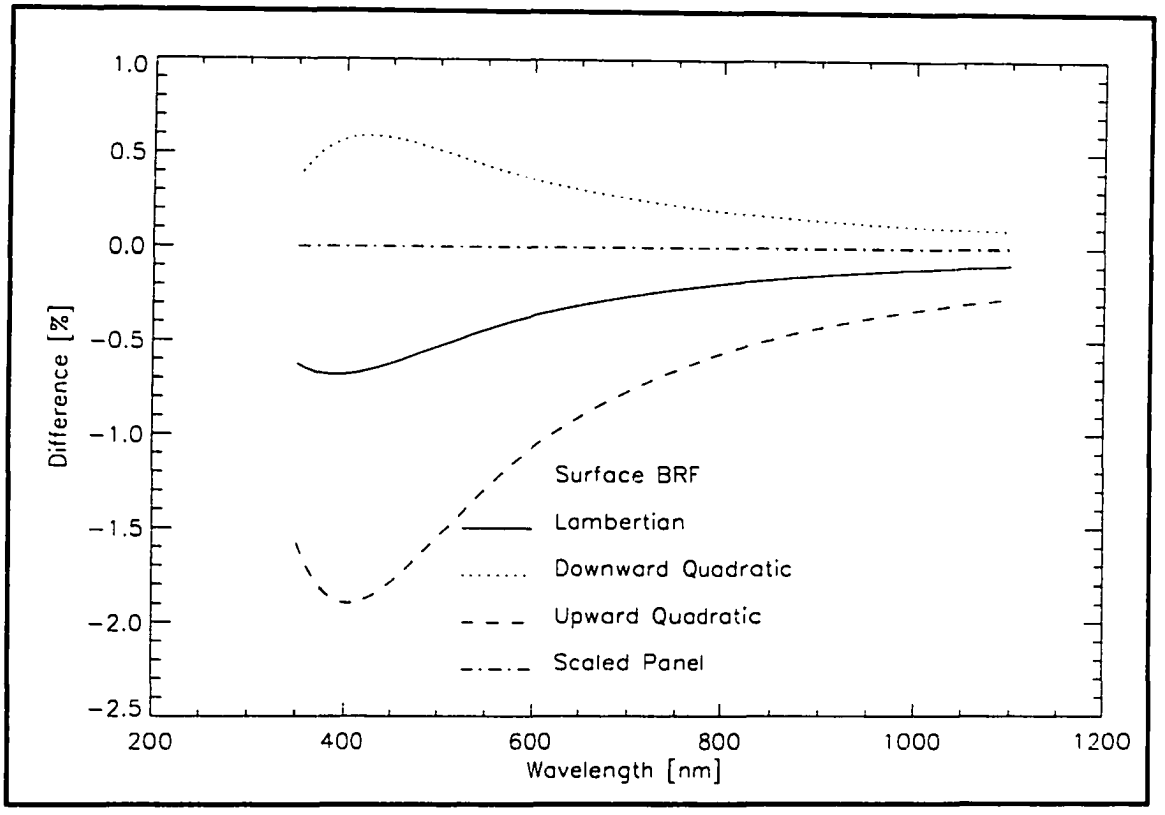


**Figure 3.7** Percent difference between $\rho_{surf}$ as calculated using Equations 3.3 and 3.4 for various underlying $BRF_{surf}$.

## Diffuse Correction Methods

The effects observed in the previous section for the theoretical cases were between 0.5% and 2%, or 0.0025 and 0.01 reflectance units at 0.5 reflectance, in the blue. This is a small effect, and for some applications it may be safe to neglect it. However, errors in the surface reflectance calculation are directly related to errors in the TOA radiance for the sensor (Biggar, 1990b). As such, making a correction for the diffuse radiance when measuring reflectance for vicarious calibration is important.

*Shaded-surface/shaded-reference method*

In order to use Equation 3.3 to find the correct value for $\rho_{surf}$, it is necessary to know $L'_{sol}$, $L_{sol}$ and $\rho_{panel}$. To measure $L'_{sol}$ or $L_{sol}$ the diffuse radiance from all directions would have to be blocked so that the spectroradiometer is viewing only the reflected solar irradiance, but this is not practical. A far easier approach to determine the reflected solar energy is to use a large parasol to block the direct solar irradiance and measure the reflected diffuse irradiance, $L'_{diff}$ or $L_{diff}$. Combining a measurement of $L'_{diff}$ and $L_{diff}$ with that of the total reflected radiances, $L'_{total}$ and $L_{total}$, allows the reflected solar energy to be determined according to

$$L'_{sol} = L'_{total} - L'_{diff}$$
$$L_{sol} = L_{total} - L_{diff} \qquad 3.10$$

which will be referred to as the shaded-surface/shaded-reference method. Therefore, the diffuse-radiance effect can be removed from the calculated surface reflectance by measuring both the reference panel and the surface while the sun is blocked with a large parasol. Then the surface reflectance is given by

$$\rho_{surf} = \rho_{panel} \frac{L_{total} - L_{diff}}{L'_{total} - L'_{diff}} \qquad 3.11$$

substituting Equation 3.10 into Equation 3.3.

The equipment needed to apply the shaded-surface/shaded-reference method include a spectroradiometer, reference panel, and parasol. After each reference measurement another

measurement is taken while the parasol is shading the reference. Similarly, data are collected after each site measurement with the parasol shading the site. The reference data are interpolated to correct for changes in the spectroradiometer response and sun angle between reference measurements. The interpolated data are used with the site data in Equation 3.11 to calculate the surface reflectance. The additional measurements required would more than double the amount of time needed to perform the data collection. Further, it would call for an additional person dedicated to the surface reflectance data collection to hold the parasol. Therefore, collecting these data is impractical.

*Shaded-reference method*

While measuring both $L_{diff}$ and $L'_{diff}$ is impractical, it is possible to measure $L'_{diff}$ with only a modest increase in the data collection time by having someone shade the reference panel for a diffuse measurement after each total reference panel measurement. If this is done, the only term missing in Equation 3.13 is $L_{diff}$. There are numerous ways to determine this term, including measuring it directly as described above. One option for determining $L_{diff}$ is

$$L_{diff} = \frac{L_{diff\text{-}RTC}}{L_{sol\text{-}RTC} + L_{diff\text{-}RTC}} L_{total} \qquad 3.12$$

where $L_{diff\text{-}RTC}$ and $L_{sol\text{-}RTC}$ are terms calculated from the RTC output and $L_{total}$ is the measured radiance from the surface. However, calculating these values requires that $BRF_{surf}$ be known and if $BRF_{surf}$ is known there is no need for this work, as the desired reflectance could be

found by simply evaluating $BRF_{surf}$ at the appropriate angles. How well $BRF_{surf}$ must be known in order to produce an accurate correction is examined later in this chapter.

Before substituting Equation 3.12 into Equation 3.11, $L'_{diff}$ must be corrected for the portion of $L_{sky}$ which is blocked by the parasol. This correction was not needed for the shaded-surface/shaded-reference method because the parasol is present for the measurement of both $L_{diff}$ and $L'_{diff}$. The magnitude of this correction can be found using barometric pressure and the Junge parameter as part of a look-up table to determine the percent change in the diffuse-to-global ratio at each wavelength. Figure 3.8 shows that for small values of $\theta_{sol}$ the correction to the diffuse-to-global ratio can approach 2% for a ratio of 0.5 and over 5% for a ratio of 0.2. The errors increase as $\theta_{sol}$ decreases because the parasol must be closer to the panel in order to shade it, which causes it to obscure a larger angular area as seen from the panel. Also, as the diffuse-to-global ratio decreases the importance of the forward scattered component increases.

The difference in the DGR is due only to errors in the measured $L'_{diff}$, so $L'_{diff}$ can be corrected by scaling by the same relative change as is seen in the DGR. A correction factor, $\Delta$, is defined as

$$\Delta = \frac{DGR_{new}}{DGR_{meas}} \qquad 3.13$$

where $DGR_{meas}$ is the measured diffuse-to-global ratio and $DGR_{new}$ is the corrected ratio. This makes the surface reflectance

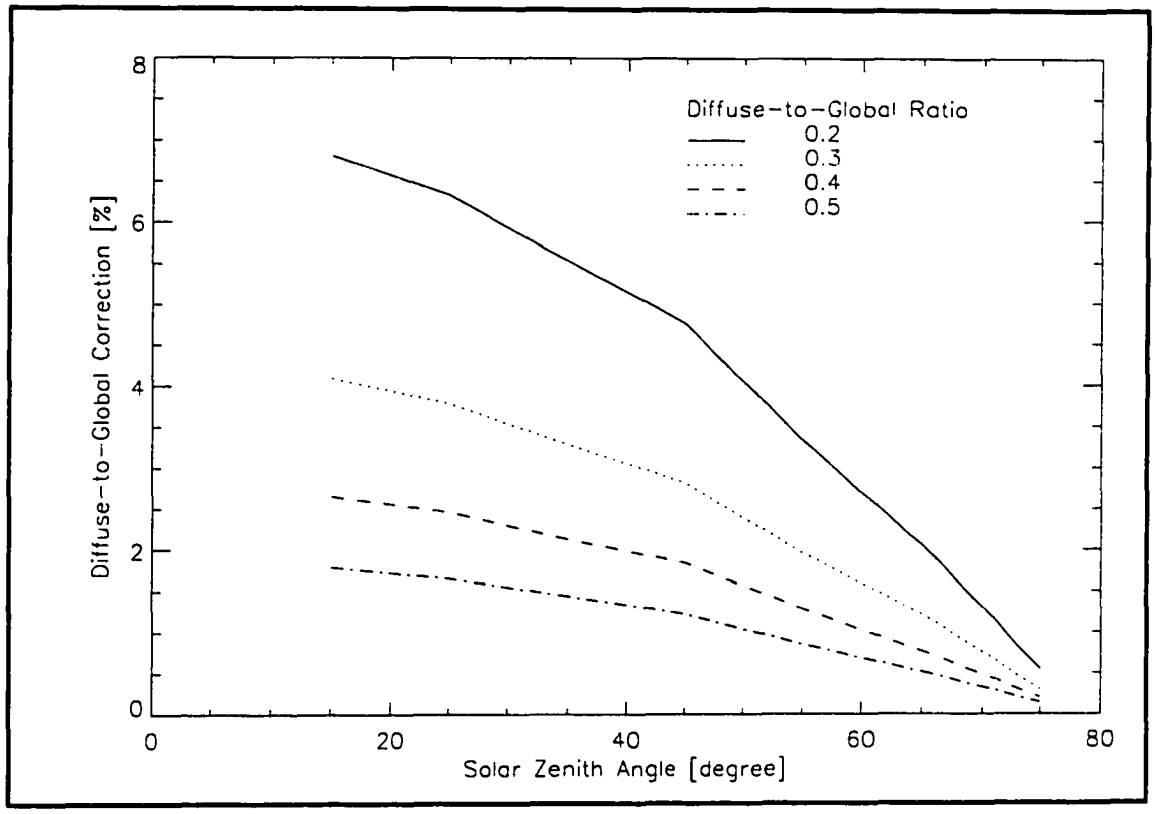


**Figure 3.8** Diffuse-to-global ratio corrections versus solar zenith angle at 350 nm for several values of the diffuse-to-global ratio.

$$\rho_{surf} = \rho_{panel} \frac{L_{total} - L_{diff}}{L'_{total} - L'_{diff}\,\Delta} \qquad 3.14$$

where $L'_{diff}\,\Delta$ is the corrected reflected diffuse radiance from the reference such that the DGR is correct. In Equation 3.14, $L_{diff}$ is calculated using Equation 3.12, and $L_{total}$, $L'_{total}$, and $L'_{diff}$ are measured quantities.

In addition to the equipment needed for the shaded-surface/shaded-reference method a solar radiometer and a barometer are needed to characterize the atmospheric properties

when applying the shaded-reference method. While surface reflectance data are collected at the test site, reflected diffuse radiance are collected of the reference after each total reflectance radiance measurement. The RTC is run using the measured atmospheric properties and the uncorrected $\rho_{surf}$ to produce the at-surface radiance field. This at-surface radiance is used to calculate the ratio of modeled radiances needed for Equation 3.13, and a code developed for use with the irradiance-based vicarious calibration method is used to calculate the corrected DGR for each wavelength. Finally, $\rho_{surf}$ is calculated using Equation 3.14.

*RTC-only method*

In cases where the parasol measurements are not made at all the RTC-only method can be applied. This method assumes that the correction for the diffuse field can be modeled as a percent change in the uncorrected surface reflectance. Later in this chapter it is shown that the percent error due to not correcting depends only on the relative shape of $BRF_{surf}$ not its absolute value. Therefore, the relative change can be calculated once and used with each calculated reflectance rather than having to evaluate the expected error each time, which reduces the computation time significantly. The correction term, $\beta$, is given by

$$\beta = \frac{\dfrac{L_{sol\text{-}RTC}}{L'_{sol\text{-}RTC}}}{\dfrac{L_{total\text{-}RTC}}{L'_{total\text{-}RTC}}} \qquad 3.15$$

where all of the radiances are calculated from RTC output based on the atmospheric properties measured at the time of the data collection. Now $\rho_{surf}$ can be written as

$$\rho_{surf} = \rho_{uncorrected}\,\beta \qquad 3.16$$

where $\rho_{uncorrected}$ is given by Equation 3.5.

The RTC-only method requires the spectroradiometer, reference panel, solar radiometer, and barometer. First the reflected total radiances are collected from surface and the reference. The RTC is then run to produce the at-surface radiance field needed to calculate the modeled radiances in Equation 3.15. Having calculated $\beta$ the correction is applied to each surface reflectance spectra collected from the site. One advantage of the RTC-only method is that it can be applied to archived data sets because it does not require any field data which is not normally collected for a vicarious calibration.

**Sensitivity to Atmospheric Properties**

The RTC used in this work calculates the scattered radiance through an iterative Gauss-Seidel method developed at the University of Arizona (Herman and Browning, 1965). The RTC separates the atmosphere into layers of equal optical depth, with the thickness of the layer being chosen such that any particular photon is unlikely to experience more than one scattering event within the layer. The RTC starts by computing the single scatter through the atmosphere, using this solution as the starting point for the iteration. Propagating towards the surface the incident term for each layer includes the attenuated solar irradiance and the downward scattered radiance from the previous layer. At the bottom of the atmosphere the downward radiance and the attenuated solar irradiance are reflected from the surface, producing the first set of upward radiances, which are then propagated back to the

top of the atmosphere in a similar manner. The process is repeated upwards and downwards through the atmosphere until the solution converges.

The proposed methods for removing the diffuse-radiance contribution, with the exception of the shaded-surface method, involve integrating the at-surface radiance field from RTC results. As such, the accuracy of the correction depends on the accuracy of the RTC itself, the accuracy of the input parameters, and the accuracy of the methods. Values for $L'_{sol}$ and $L_{sol}$, the reflected radiances due to the directly-transmitted solar irradiance, and $L'_{diff}$ and $L_{diff}$, the reflected radiances due to downwelling sky irradiance, were produced using RTC output with the inputs listed in Table 3.1. The reference panel was assumed to be spectrally flat with non-lambertian properties typical of the RSG site panel, and the surface BRF was assumed to be lambertian with a 0.5 reflectance. The RTC was then used to calculate a perturbed diffuse irradiance by changing the value of one of the input parameters. The shaded-reference and RTC-only methods were applied to the modeled reflected radiances using the perturbed diffuse irradiance in order to determine the methods' dependency on each input.

The inputs perturbed included the real and imaginary parts of the complex index of refraction, the Junge parameter, the aerosol optical depth, the barometric pressure, surface elevation, and the surface reflectance. In each case, the input was varied by an amount greater than the expected error for that input and the affect on the diffuse correction methods was found to be on the order of 0.05% or less. However, when the surface BRF used with the diffuse corrections differed from the BRF used to produce the reflected radiances the

calculated surface reflectance changes by 0.5% through 2%. Therefore, the dependency on the assumed value of the surface BRF is examined in more detail.

**Surface BRF Dependence**

The shaded-reference and RTC-only methods presented here for correcting $\rho_{surf}$ for the diffuse radiance component depend on a knowledge of the surface BRF and the reference panel BRF. $BRF_{panel}$ is known from laboratory measurements, while $BRF_{surf}$ must be measured in the field or estimated. Errors in the $BRF_{surf}$ used will lead to errors in the retrieved $\rho_{surf}$.

*Absolute magnitude of $BRF_{surf}$*

The diffuse correction methods both use a ratio of modeled values to correct for the diffuse field. Because these ratios assume the same BRF in both numerator and denominator, the $BRF_{surf}$ used for the correction can be scaled by a multiplicative factor without changing the value of the correction. This is a very useful trait for the correction method because changes in the absolute reflectance with wavelength or position within the site will not adversely effect retrieval. Further, the insensitivity to scaling implies that while the relative shape of $BRF_{surf}$ needs to be known, the absolute magnitude does not.

*Dependence of $L_{total}$ on $BRF_{surf}$*

The goal of the correction methods is to determine the values $L_{sol}$ and $L'_{sol}$ from measured values of $L_{total}$ and $L'_{total}$ and combinations of measured and modeled values for $L_{diff}$ and $L'_{diff}$. Therefore, understanding the affect of $BRF_{surf}$ on $L_{total}$ will provide insight into the importance of $BRF_{surf}$ to the corrections. It is useful to first look at a simplified case where

$$BRF_{surf}(\theta_{inc},\phi_{inc};0°,0°) = constant$$
$$L_{sky}(\theta_{inc},\phi_{inc}) = constant \qquad 3.17$$

that is, the surface is lambertian and the diffuse radiance field is isotropic. For this case, the integration in Equation 3.2 can be done analytically giving $L_{diff}$ as

$$L_{diff} = BRF_{surf}\, L_{sky}\, \sin^2\theta\,|_0^{\frac{\pi}{2}} = BRF_{surf}\, L_{sky} \qquad 3.18$$

or it can also be written with $-\cos^2\theta$. The relative importance of $BRF_{surf}$ at different zenith angles can be examined by separating the integral into a sum of the integrals over 10° sections in zenith angle. Figure 3.9 plots the ratio of the reflected diffuse radiance from a 10° annulus at a particular incident angle $\theta$ to the reflected total radiance for diffuse-to-global ratios (DGR) of 0.45 and 0.15. The contribution of the diffuse light at incident zenith angles greater than 80° are 1.36% and 0.45% for DGRs of 0.45 and 0.15. It is fortunate that the contributions due to radiances near the horizon are so small because the errors in the calculated radiance and the measured $BRF_{surf}$ are largest near the horizon.

The actual $L_{sky}$ encountered is not isotropic because the scattered radiance increases as $\theta$ approaches the horizon due to the increase in the path length and because the aerosol scattering produces a strong forward peak around the solar angles. The exact effect of these two processes are dependent on the atmospheric properties and the incident solar zenith angle. $L_{diff}$ and $L_{total}$ were calculated using $L_{sky}$ output from the RTC for the atmospheric properties listed in Table 3.1, a 30° solar zenith angle, and a lambertian surface. Figure 3.10

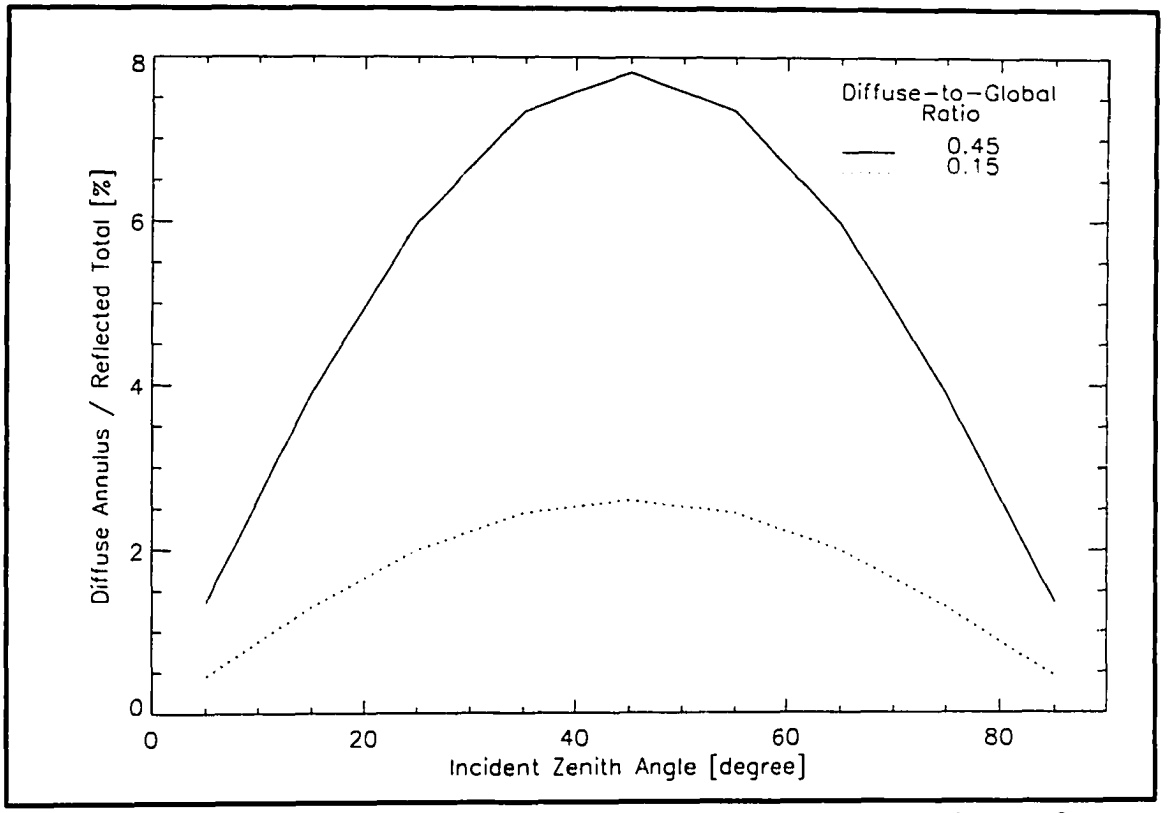


**Figure 3.9** Percent of reflected total radiance contributed by diffuse light from 10° annuluses for a lambertian surface and isotropic radiance field.

plots the percent contribution of 10° annuluses to $L_{total}$ at 350 nm and 500 nm, which correspond to DGRs of approximately 0.45 and 0.15 as in Figure 3.9. Because of the directional nature of $L_{sky}$ the percent of the reflected total radiance due to diffuse light from incident zenith angles greater than 80° has now increased to 1.88% and 1.28% for 350 nm and 500 nm, respectively. While these contributions are still small, they are becoming more significant. Further these contributions will increase with increasing solar zenith angle because the DGR is greater at large sun angles.

The affect of near-horizon radiances was also examined using $BRF_{surf}$ typical of Ivanpah Playa with the same $L_{sky}$ used above. The addition of a non-constant $BRF_{surf}$ changes

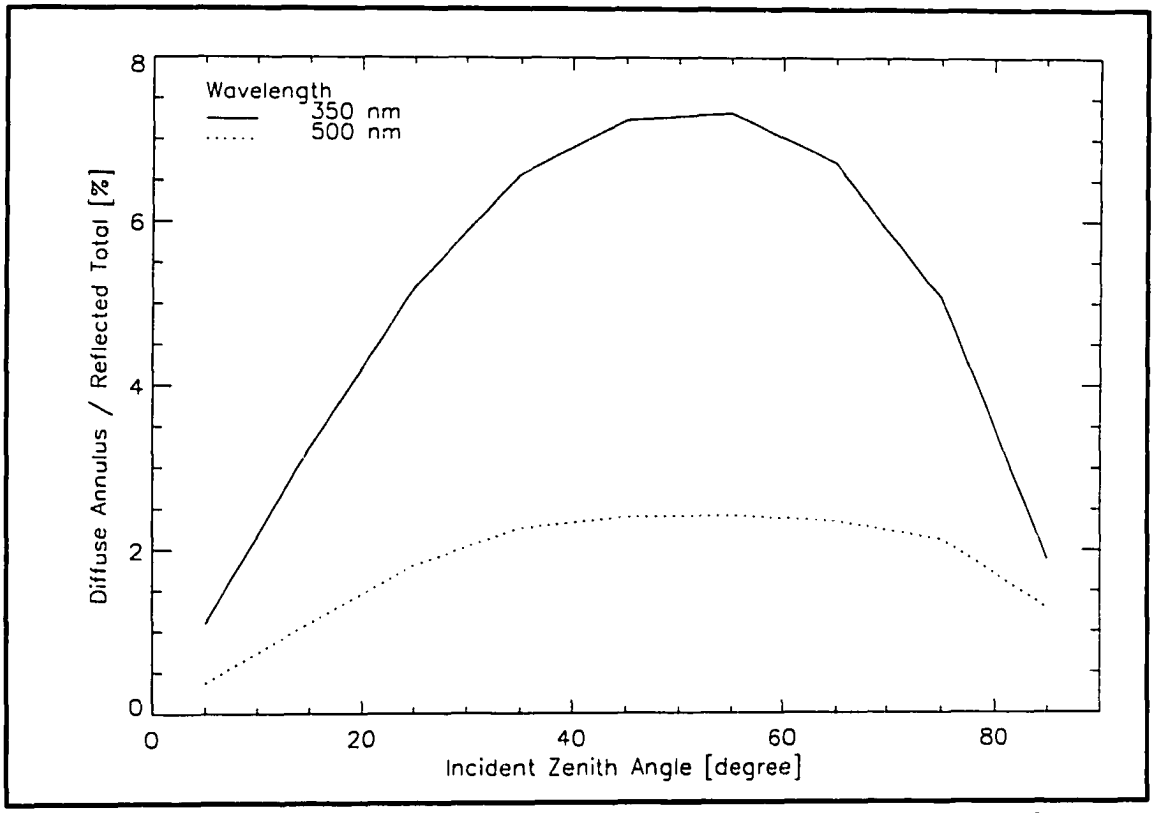


**Figure 3.10** Percent reflected total radiance contributed by diffuse light from 10° annuluses for a lambertian surface and real radiance field.

the contribution of diffuse radiance from incident zenith angles greater than 80° by less than 0.1% at a solar zenith angle of 30°.

The portion of the reflected total radiance which is due to incident irradiance from near the horizon is on the order of 1%, and errors in either the radiance or the BRF near the horizon will not produce large errors in the calculation of $L_{total\text{-}RTC}$. However, because the error which is being corrected is normally on the order of 1% or 2% as well, these errors can not be ignored when applying the diffuse correction methods.

*Correcting assuming a lambertian surface*

If there are no measurements of $BRF_{surf}$ available to use with the correction methods, one possibility is to use the known properties of the reference panel and assume the surface is lambertian. Radiance data were produced from RTC output which assumed a spectrally flat hemispherical reflectance of 0.5 which followed the shape of the BRF for Ivanpah Playa (Nandy, 2000). The reference used followed the BRF measured for the RSG's site panel and was spectrally flat, as well. Figure 3.11 is a plot of the percent error from the correct nadir-view reflectance at 350 nm versus solar zenith angle. The solid line is the percent error due to assuming a lambertian $BRF_{surf}$ for the correction, and the dotted line is the percent error of not correcting.

To understand the large changes in the reflectance errors shown in Figure 3.11 it is necessary to consider the effective $BRF_{surf}$ for each solar angle. It was shown in Figure 3.7 that if $BRF_{surf}$ is a constant times $BRF_{panel}$ then there is no error incurred by not correcting for the diffuse light. Not correcting can therefore be viewed as correcting assuming a $BRF_{surf}$ which is the same as $BRF_{panel}$ times a constant. Setting Equations 3.10 and 3.3 equal to each other the constant is found such that

$$BRF_{surf} = \frac{L_{total}}{L'_{total}} BRF_{panel} \qquad 3.19$$

where ratio of the reflected total radiances is evaluated at each wavelength. Figures 3.12 and 3.13 are plots of $BRF_{surf}$ for Ivanpah and the effective $BRF_{surf}$ for a lambertian correction, $BRF_{lamb}$, and not correcting, $BRF_{nocorr}$, for a solar zenith angles of 35° and 60° respectively.

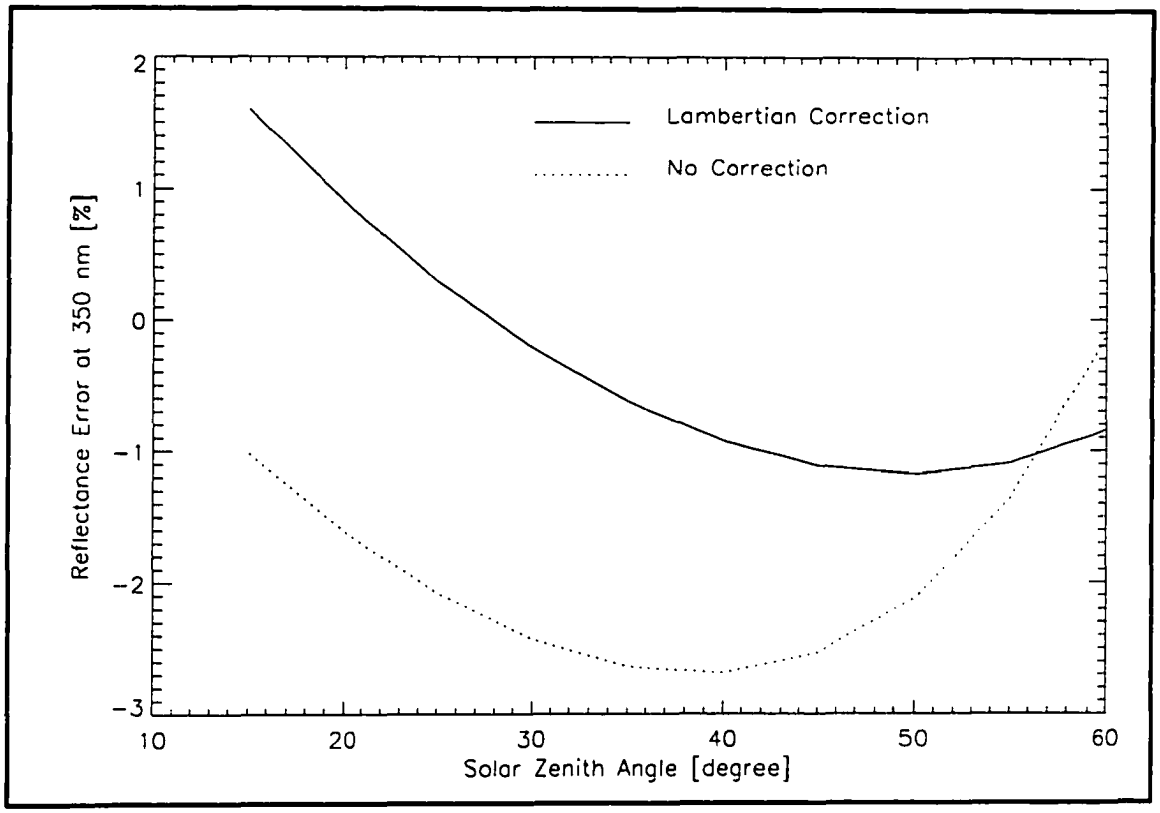


**Figure 3.11** Reflectance error at 350 nm versus solar zenith angle for no correction and correcting using a lambertian $BRF_{surf}$.

In Figure 3.12 $BRF_{nocorr}$ is seen to underestimate $BRF_{surf}$ which leads to a smaller effective value of $L_{diff}$. Reducing $L_{diff}$ in Equation 3.9 causes the uncorrected value of $\rho_{surf}$ to be greater than the real value, which is what is observed. In Figure 3.13, $BRF_{uncorr}$ more nearly overestimates and underestimates $BRF_{surf}$, which is why the error for not correcting is so small.

When the only errors in the correction methods are due to an incorrect $BRF_{surf}$ both methods display identical dependence on $BRF_{surf}$, though the explanation for the errors differ. The RTC-only method calculates a correction term to $\rho_{uncorrected}$, so the errors are a result of whether the differences between $BRF_{surf}$ and $BRF_{nocorr}$ are the same as the differences

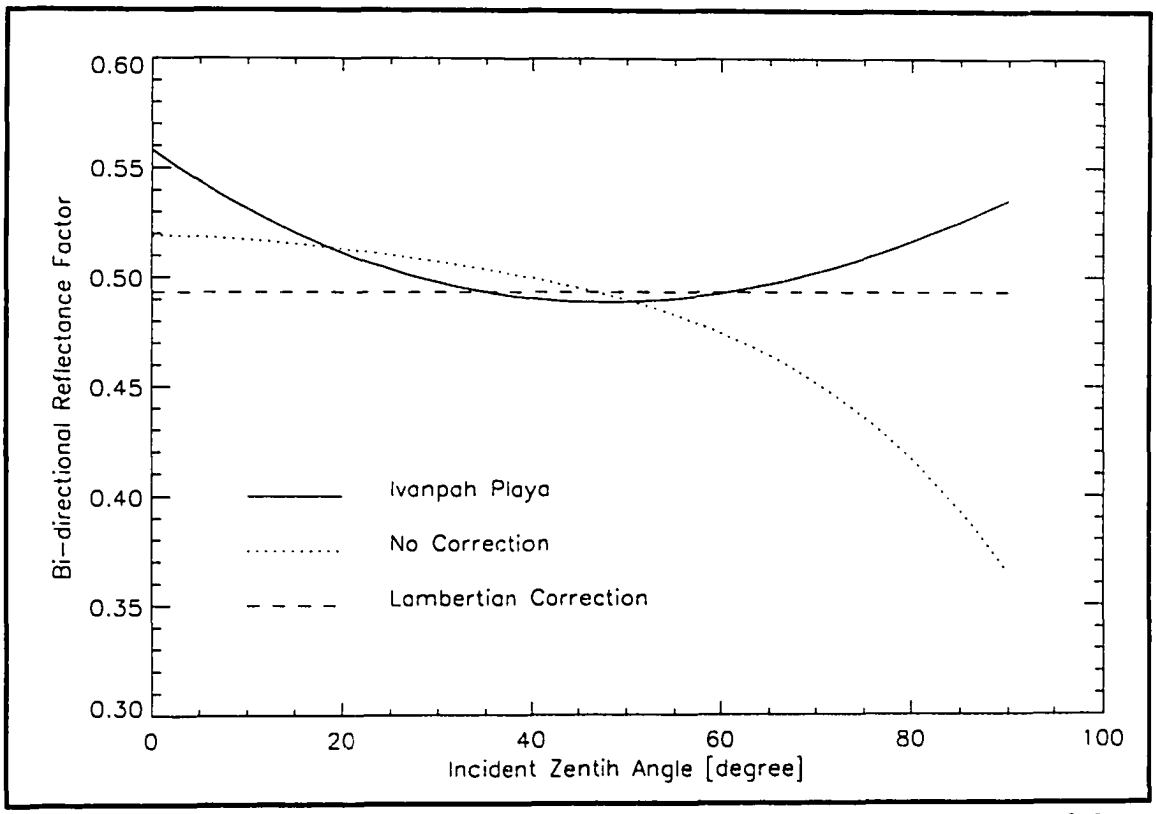


**Figure 3.12** Bi-directional reflectance factor functions at a solar zenith angle of 35° for Ivanpah Playa, no correction, and a lambertian surface correction.

between $BRF_{lamb}$ and $BRF_{nocorr}$. At a solar zenith angle of 35° the difference between $BRF_{lamb}$ and $BRF_{nocorr}$ almost compensate for the difference between $BRF_{surf}$ and $BRF_{nocorr}$, while at 60° the differences are such that the RTC-only method 'corrects' $\rho_{uncorr}$ away from the right answer rather than towards it.

The assumption inherent to the shaded-reference method is that the ratios $L_{diff}/L_{total}$ and $L_{diff\text{-}RTC}/L_{total\text{-}RTC}$ are equal. Since $BRF_{surf}$ can be multiplicatively scaled without changing the magnitude of the correction, it is easiest to think of $BRF_{lamb}$ and $BRF_{surf}$ as having the same value at $\theta_{sol}$, because with this scaling $L_{sol}$ and $L_{sol\text{-}RTC}$ are equal, and the errors are due only to the relative values of $L_{diff}$ and $L_{diff\text{-}RTC}$. At both solar zenith angles $BRF_{lamb}$

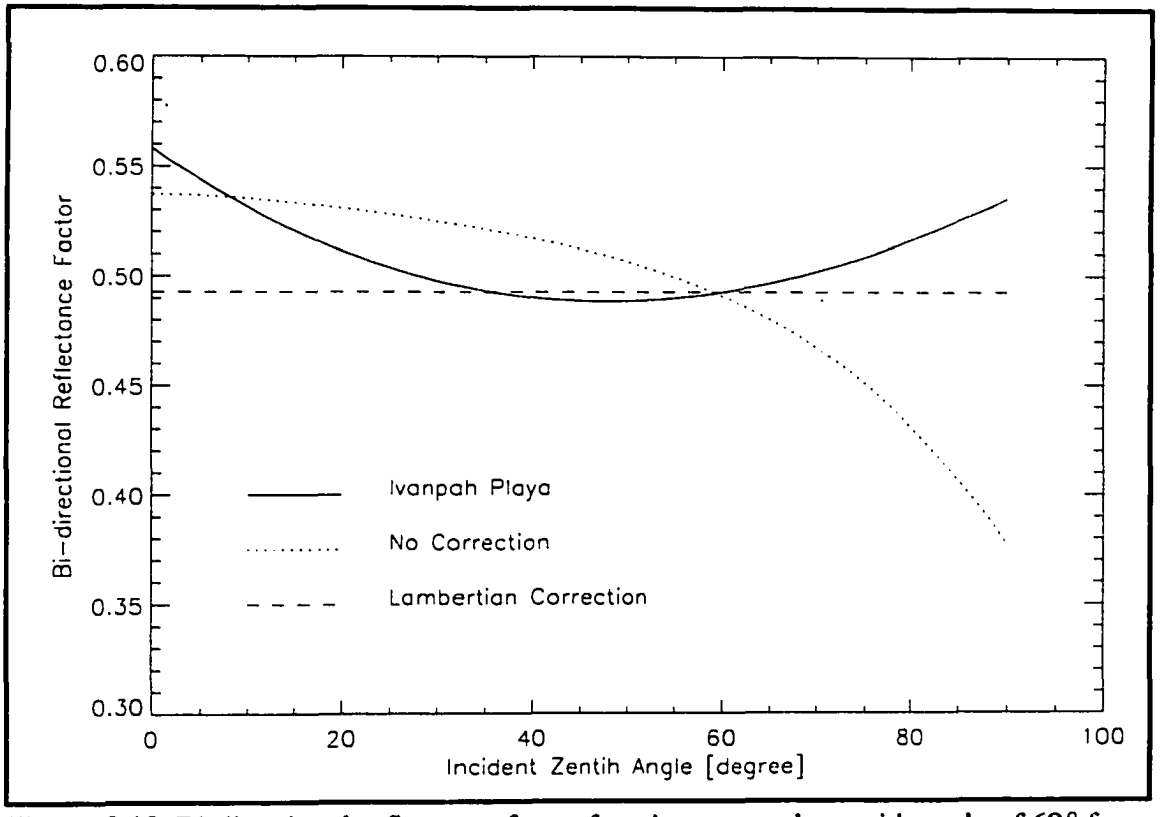


**Figure 3.13** Bi-directional reflectance factor functions at a solar zenith angle of 60° for Ivanpah Playa, no correction, and a lambertian surface correction.

underestimates $L_{diff}/L_{total}$ by about the same amount, and as expected the error in the correction is also about the same.

*Correcting using actual $BRF_{surf}$ with a linear bias*

The measurement of BRF is hardest at large angles, and consequently the errors in $BRF_{surf}$ tend to be larger near the horizon. These types of errors are simulated by using $BRF_{error}$ such that

$$BRF_{error}(\theta_{inc},\phi_{inc}) = BRF_{surf}(\theta_{inc},\phi_{inc}) \qquad \theta < 60°$$

$$BRF_{error}(\theta_{inc},\phi_{inc}) = BRF_{surf}(\theta_{inc},\phi_{inc}) * \left(1 + \frac{\theta_{inc} - 60°}{30°} \epsilon\right) \qquad \theta \geq 60° \qquad 3.20$$

where $\epsilon$ is total percent bias at an incident zenith angle of 90°. $BRF_{error}$ was used to correct simulated data from Ivanpah Playa, and the value of $\epsilon$ was incremented by 1% steps, until the maximum of the magnitude of the error in the retrieved reflectance was 0.01 reflectance units (~2%). Using this method it was found that the retrievals maintain accuracy to better than 0.01 reflectance units for an $\epsilon$ of ±25% for solar zenith angles between 15° and 60°.

Since the values for $BRF_{surf}$ will not be known perfectly for incident zenith angles less than 60°, a study similar to the above was performed where the linear bias was over the entire range of incident zenith angles. $BRF_{error}$ is now given by

$$BRF_{error}(\theta_{inc},\phi_{inc}) = BRF_{surf}(\theta_{inc},\phi_{inc}) \left(1 + \frac{\theta_{inc}}{90°}\epsilon\right) \qquad 0° \le \theta_{inc} \le 90° \qquad 3.21$$

where $\epsilon$ is still the maximum bias at an incident zenith angle of 90°. Because $BRF_{error}$ has an error at the solar zenith angle, it is the deviations of $BRF_{error}$ relative to the value at the solar zenith angle which determine the error in the retrieved reflectances. For instance, when the solar zenith angle is 45° $BRF_{error}$ is biased to a higher value at incident angles less than 45° and to a lower value at angles greater than 45°. Because the bias is linear, the BRF errors would cancel exactly if $L_{sky}$ were isotropic. Using $BRF_{error}$ with the correction methods, an $\epsilon$ of ±25% will still be sufficient for solar zenith angles between 35° and 60°. However, for solar zenith angles less than 35° the allowable $\epsilon$ decreases, and for an angle of 15° an $\epsilon$ of ±13% is needed to maintain an accuracy of 0.01 reflectance units.

*RTC-only method using a molecular-only atmosphere*

In cases where $BRF_{surf}$ is not known to within 20% at angles near the horizon, one possibility for correction is to use the RTC-only method with an atmosphere that exhibits only molecular scattering. In a molecular-only atmosphere the total amount of scattering will be smaller and $L_{sky}$ will be more uniform because molecular scattering does not have a forward scatter peak. Therefore, using only the molecular scattering will tend to under correct the surface reflectance. A molecular only atmosphere can not be used with the shaded-reference method, because doing so would cause significant biases because $L'_{diff}$ is measured under the actual illumination conditions.

Figure 3.14 plots the percent error in the reflectance due to not correcting and due to correcting using a molecular-only atmosphere for a solar zenith angle of 35°. As was expected the correction has reduced the error in the surface reflectance, but not fully corrected for it. Since the molecular-only atmosphere reduces the affect of the diffuse radiance using $BRF_{error}$ from Equation 3.21 with $\epsilon$ positive causes the percent bias which produces and error of 0.01 reflectance units to increased to greater than 45% for solar zenith angles between 15° and 60°. However, when $\epsilon$ is negative the errors due to using $BRF_{error}$ are of the same sign as errors due to the molecular-only atmosphere and for solar angles between 25° and 50° the allowable size of $\epsilon$ is decreased. Because the goal of using a molecular-only atmosphere was to reduce the dependance on $BRF_{surf}$ near the horizon and the sign of errors in $BRF_{surf}$ will not be known, using a molecular-only atmosphere is not recommended.

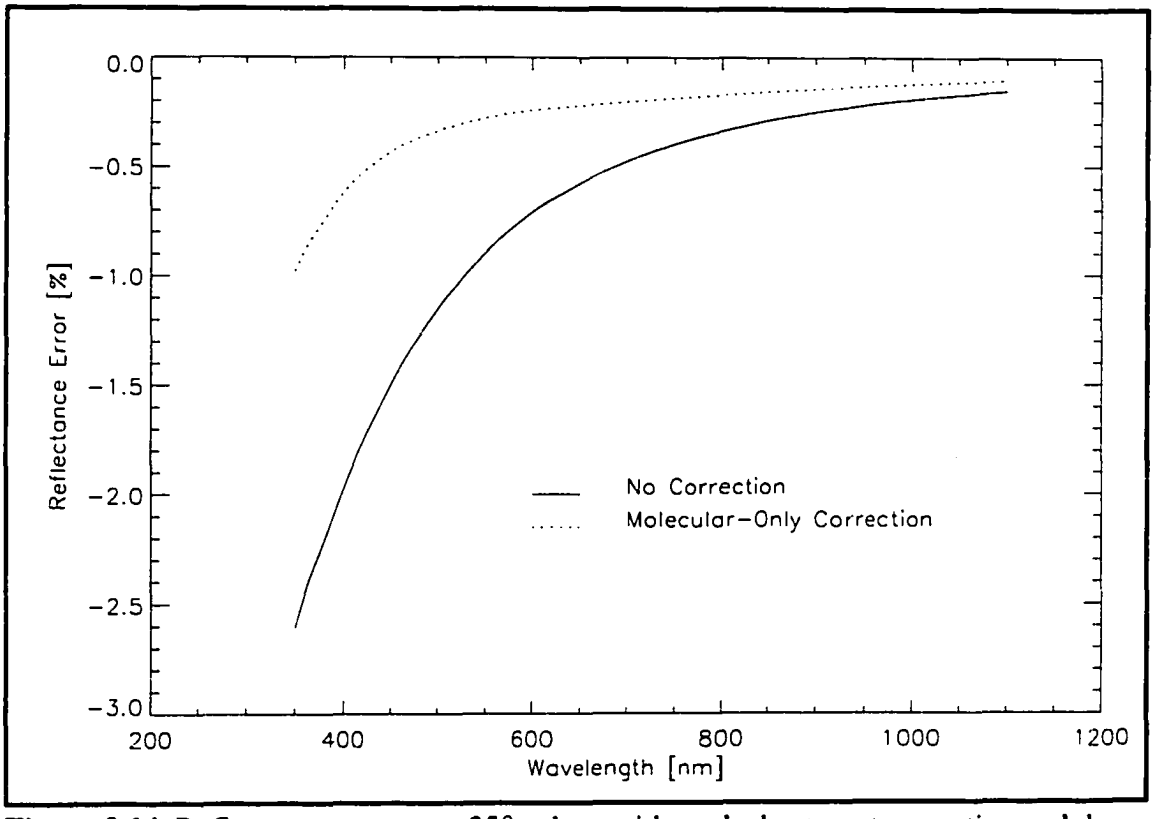


**Figure 3.14** Reflectance errors at a 35° solar zenith angle due to not correcting and due to correcting with a molecular-only atmosphere.

*Other Calibration Sites*

Simulated data similar to that described above were produced for two other calibration sites regularly used by the RSG, White Sands Missile Range and Railroad Valley Playa. Figure 3.15 plots $BRF_{surf}$ for each of the three sites normalized to a hemispherical reflectance of 0.5. In both cases, the dependence on linear biases in $BRF_{surf}$ at all incident zenith angles and at only zenith angles greater than 60° were found to be almost identical to the results for Ivanpah Playa.

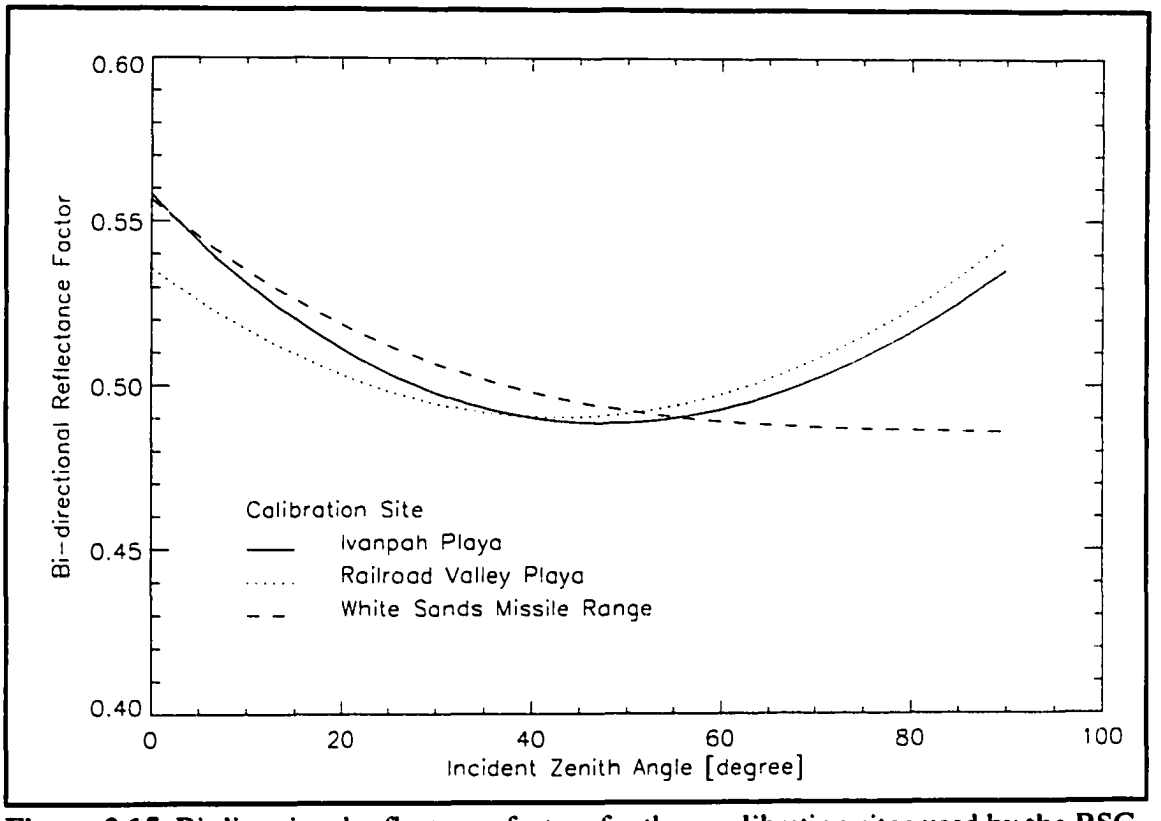


**Figure 3.15** Bi-directional reflectance factors for three calibration sites used by the RSG normalized to a hemispherical reflectance of 0.5.

## Conclusions

When measuring surface reflectance in the field the differences between the directional-directional and the hemispherical-directional reflectances can be significant. The magnitude of the error will depend on $BRF_{surf}$, the atmospheric properties, and the solar zenith angle, and can exceed 2% for the sites used by the RSG. Therefore, it is suggested that one of the above corrections for the diffuse radiance be applied to field reflectance data.

The shaded-surface/shaded-reference method is the most accurate correction method presented. By measuring $L_{total}$, $L'_{total}$, $L_{diff}$, and $L'_{diff}$ it is possible to retrieve the directional-directional reflectance using Equation 3.11. This method does not require any assumptions

about the nature of $BRF_{surf}$ or $L_{sky}$, and as such, the accuracy is dependent on the stability and accuracy of the spectroradiometer and on the calibration of the reference panel. Thus, this correction method can be applied even in instances where the expected error is less the 2% limit imposed above, however, the additional time and personnel required to collect the data for this method make it unlikely that it will be applied on a regular basis.

The shaded-reference and RTC-only methods provide corrections for the diffuse radiance with little or no additional data collection. Both methods rely on some prior knowledge of the relative shape of $BRF_{surf}$, but not the absolute magnitude. In cases where the BRF at zenith angles less than 60° is well known, linear biases above 60° can be as large as 25% at a zenith angle of 90° without introducing errors in excess of 2% for all solar zenith angles. If $BRF_{surf}$ is not well known for angles less than 60° a bias at 90° of less than 25% will still be sufficient for solar zenith angles between 35° and 60°, but for solar zenith angles less than 35° the allowable linear bias is reduced to approximately 15%.

While the shaded-reference method has the potential to be more accurate, any differences between the actual and the predicted at-surface radiance, for instance due to clouds or buildings, will cause large errors. Because the RTC-only method uses only modeled data for the reflected diffuse radiances, such differences will have a much smaller impact than when modeled and measured values are both used. Therefore, in any case where there are clouds or other obstructions present, the RTC-only method is preferable.

# CHAPTER 4

# DIFFUSE CORRECTION APPLIED TO REAL DATA SETS

The modeled data sets in Chapter 3 established the reliability and limitations of the diffuse corrections. The corrections have now been applied to data sets collected using the RSG's standard field equipment. Data were collected on 3 March 2000 and 3 July 2000 viewing three reflectance tarpaulins with nominal reflectances of 2%, 8% and 48%. Reflected total and diffuse radiances were measured for the reference and the tarpaulins which allowed all three diffuse corrections to be performed. Further, the BRF's of the tarpaulins were measured in the laboratory according to the methods described in Appendix A, providing a correct baseline for comparison of the models.

Other data were collected on 28 October 1999 at White Sands Missile Range in Alamagordo, New Mexico. These data included upwelling radiance measurements of the reference panel and surface, both shaded and unshaded. Using these measurements the shaded-surface/shaded-reference, shaded-reference and RTC-only diffuse correction methods were applied to calculate surface reflectances for the site.

## Reflectance Tarpaulin Measurements

On 3 March 2000 and 3 July 2000 data were collected in the parking lot of the RSG building in Tucson, AZ. The equipment used for the data collections included a commercially available spectroradiometer, a 10-band automated solar radiometer, a digital barometer/thermometer, and the RSG's 46-cm Spectralon diffuser used as a reference. The data from the solar radiometer were used with the pressure and temperature to calculate the molecular and aerosol optical depths as well as the ozone density for input to the RTC. The

spectroradiometer was used to collect the upwelling reflected radiances from the reference and from the tarpaulins.

On 3 July 2000 the skies were clear near the sun, but there were clouds to the west which grew thicker as the morning progressed. On 3 March 2000 the weather was clear but the tarpaulins orientation was not properly taken into account, making comparisons to the laboratory data difficult. The clouds on 3 July 2000 cause a greater contribution due to the diffuse radiance because of they are brighter than clear sky and because their edges represent discontinuities in the diffuse radiance field. Since the RTC output used for the shaded-reference and RTC-only methods does not include the effects due to clouds, the data from 3 July 2000 will be presented to demonstrate the accuracy of the shaded-surface/shaded-reference method even in adverse conditions, and the shaded-reference and RTC-only results from 3 March 2000 will be compared to the shaded-surface/shaded-reference data from that day.

*Reflectance Tarpaulin Characterization*

The BRF of the reflectance tarpaulins used for this experiment were characterized in the goniometric facilities of the RSG. The reflectance tarpaulins are approximately 61 cm to a side and were cut from the material provided by the manufacturer for repairs to larger tarpaulins (approximately 7 m square). The repair material had been stored rolled up, which resulted in creases. Also, the weave of the tarpaulins is such that the stitches are aligned in one orientation and offset in the other. The creases are parallel to the aligned stitches for all three tarpaulins. Because of the creases and weave the tarpaulins were measured twice, once with the creases aligned vertically, and again after the tarpaulin was rotated 90°.

When the tarpaulin is aligned vertically, the creases cast shadows as the incident angle increases, which in turn lowers the measured BRF at those angles. The effect of the material's weave is just the opposite. When the aligned rows of stitches are vertical, the principle plane of the measurement is such that the light is being reflected from long uniform lines. This reflectance is more efficient than the other orientation where the light is scattered more because of the irregular nature of the weave.

Figure 4.1 shows the BRF as a function of incident zenith angle at 554 nm for the 48% reflectance tarpaulin with the creases horizontal and vertical and Figure 4.2 shows the vertical and horizontal orientation BRF's for the 8% and the 2% reflectance tarpaulins. Examination of the tarpaulins reveals that the creases for the 48% tarpaulin are the least severe, and so it is the nature of the weave which dominates its behavior. The 2% and the 8% tarpaulins have more pronounced creases and so their behavior is a combination of both the shadows and the weave.

Both Figures 4.1 and 4.2 demonstrate that the orientation reflectance tarpaulins significantly effect the BRF. This orientation dependency effect the experiment in two distinct ways. First, when measuring the tarpaulins outside care must be taken to align them with the principle plane of the sun or the correct value for the BRF will not be known. Second, the shaded-reference and the RTC-only methods assume that $BRF_{surf}$ has no azimuthal dependance. Because the tarpaulins are clearly not symmetric in azimuth, $BRF_{surf}$ was taken to be the average of the two orientations, so that the errors introduced will tend to cancel.

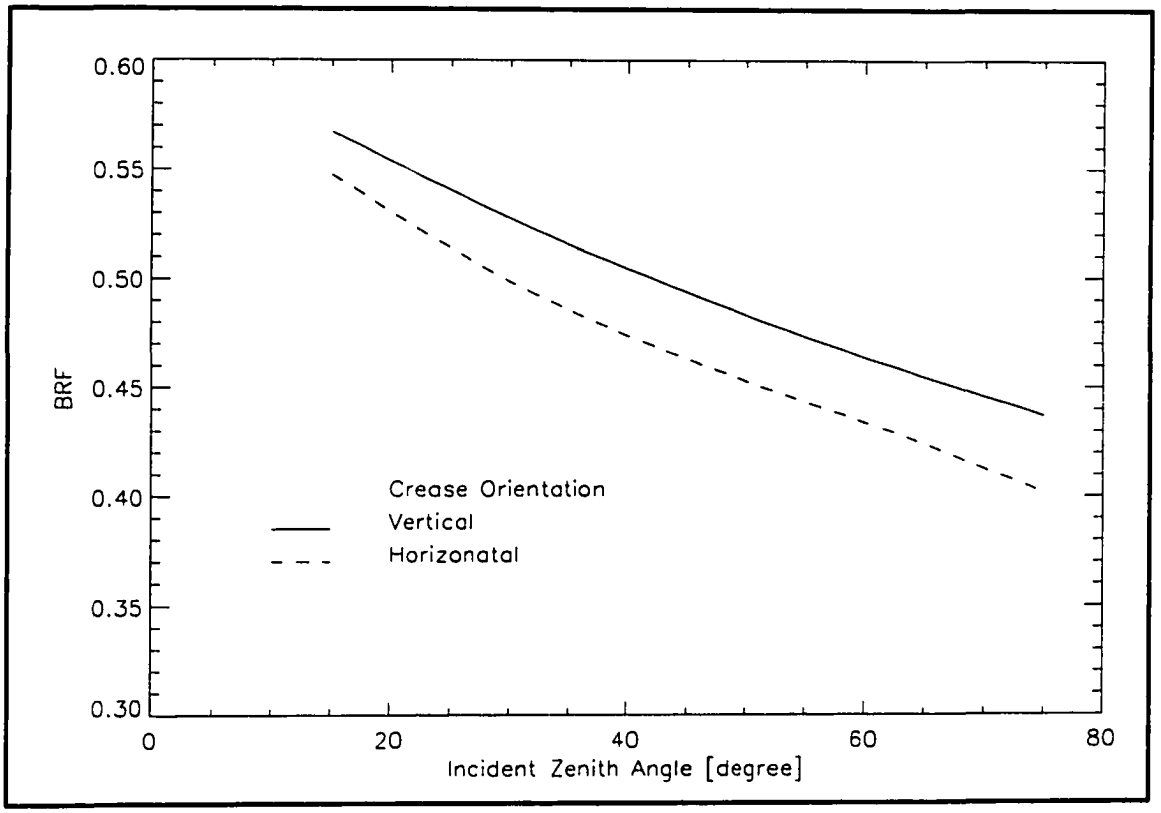


**Figure 4.1** BRF of a 48% reflectance tarpaulin at 554 nm with creases horizontal and vertical with respect to the optical axis.

*Experimental setup for 3 July 2000*

The pistol grip for the spectroradiometer with the 8° field of view fore-optic was attached to the end of a boom arm on a tripod and the spectroradiometer was configured to average 20 spectra for each file saved. The spectroradiometer reports digital numbers at 1 nm intervals from 350 nm through 2500 nm, using three separate detectors to cover the wavelength range. Since the scattered radiance field drops off sharply with increasing wavelength, only the VNIR data(350 nm - 1100 nm) is presented throughout this chapter.

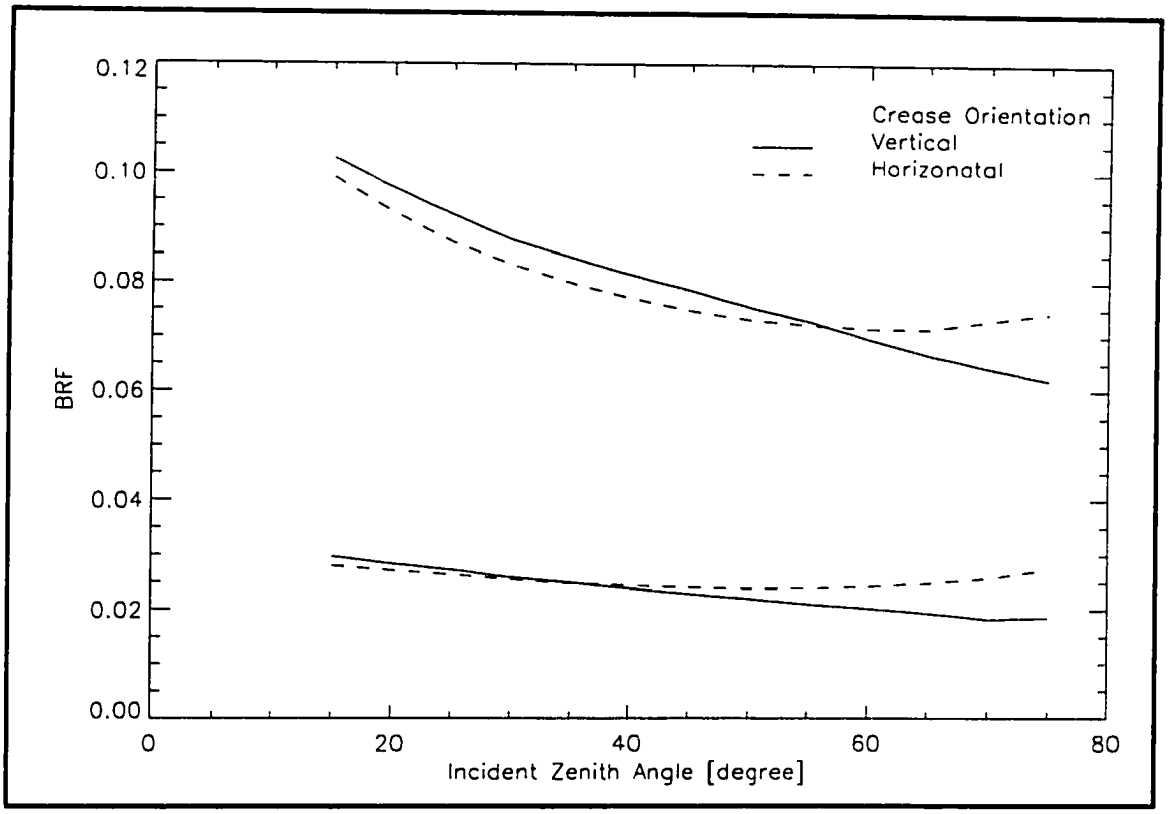


**Figure 4.2** BRF for the 2% and 8% reflectance tarpaulins with the creases horizontal or vertical with respect to the optical axis.

Figure 4.3 shows the set-up, including the spectroradiometer, reference, reflectance tarpaulin, and parasol. The parasol used is a square piece of sheet metal approximately 76 cm to a side and is mounted to a pole with an adjustable head which allows the angle of the parasol to be set such that it is normal to the directly transmitted solar irradiance. The person holding the parasol attempts to crouch down as low as possible, in order to minimize light being reflected from the person directly onto the reference or tarpaulin and to minimize the amount of diffuse light obstructed.

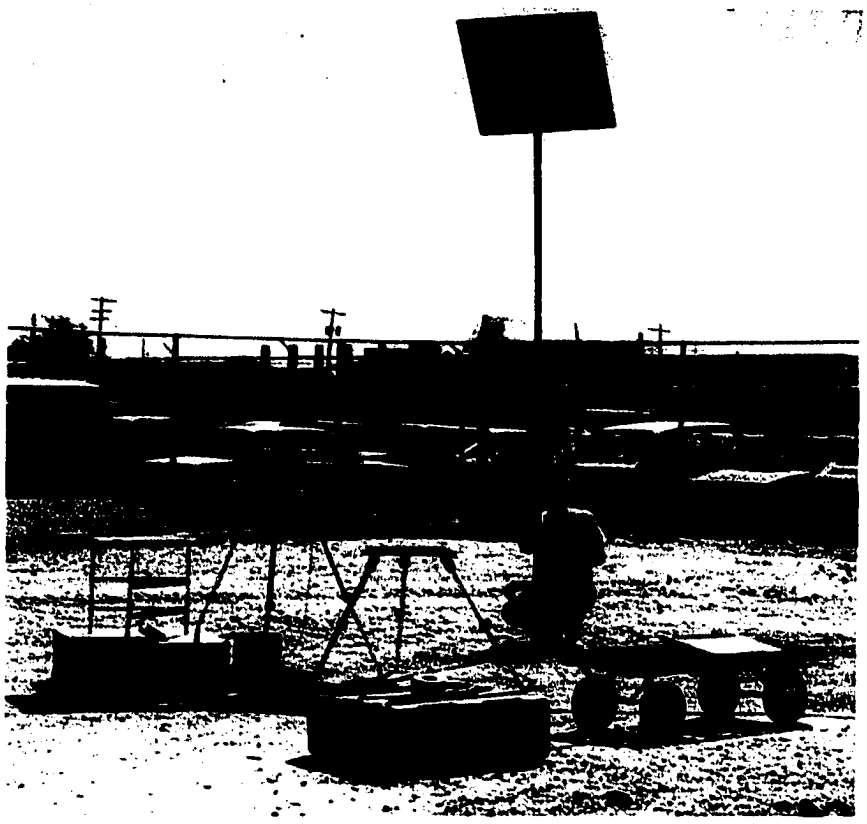

**Figure 4.3** Experimental set up in RSG's parking lot on 3 March 2000.

The procedure for data collection was as follows. The reference panel and reflectance tarpaulin were aligned to the sun's principle plane and leveled. The tarpaulins were positioned such that the aligned rows of stitches were lying along the principle plane, which corresponds with the creases being horizontal in the blacklab measurements. The spectroradiometer was then optimized on the reference, and $L'_{total}$ was measured. The parasol was held in place to shade the reference and $L'_{diff}$ was measured. The boom arm was then rotated so that the spectroradiometer was viewing the tarpaulin and measurements of $L_{total}$ and $L_{diff}$ were collected. Finally, the boom arm was rotated back and a second measurement was made of $L'_{total}$ and $L'_{diff}$. Whenever the input changed dramatically, either from shading

or rotating the boom arm, the spectroradiometer was allowed to run through at least one average of 20 spectra before data were collected. This was done to avoid spectra in the data which included two different inputs in the average. This procedure was repeated for all three tarpaulins and for solar zenith angles of approximately 60°, 50°, and 40°.

*Results for 3 July 2000*

The calibration sites used by the RSG generally have surface reflectances of approximately 0.5, therefore the results for the 48% reflectance tarpaulin will be examined in some detail. The reflectance of the tarpaulin for a solar zenith angle of 40.1 ° is plotted versus wavelength in Figure 4.4 The solid line is the uncorrected value, the dotted line is the value corrected with the shaded-surface/shaded-reference method, and the diamonds are the values from the laboratory. Figure 4.5 plots the error of the uncorrected and the corrected reflectances evaluated at the discrete wavelengths measured in the laboratory. Both the uncorrected and the corrected reflectances have large errors at 400 nm. These errors are likely due to the rapidly changing reflectance, such that at 400 nm a 1 nm error in the spectral calibration results in an error in the reported surface reflectance of greater than 0.009 reflectance units.

There is also an anomalous point near 650 nm, which can be seen in both Figures 4.4 and 4.5. Between 625 nm and 675 nm the uncorrected reflectance dips, while the reflectance calculated using the shaded-surface/shaded-reference method is flatter. For the laboratory

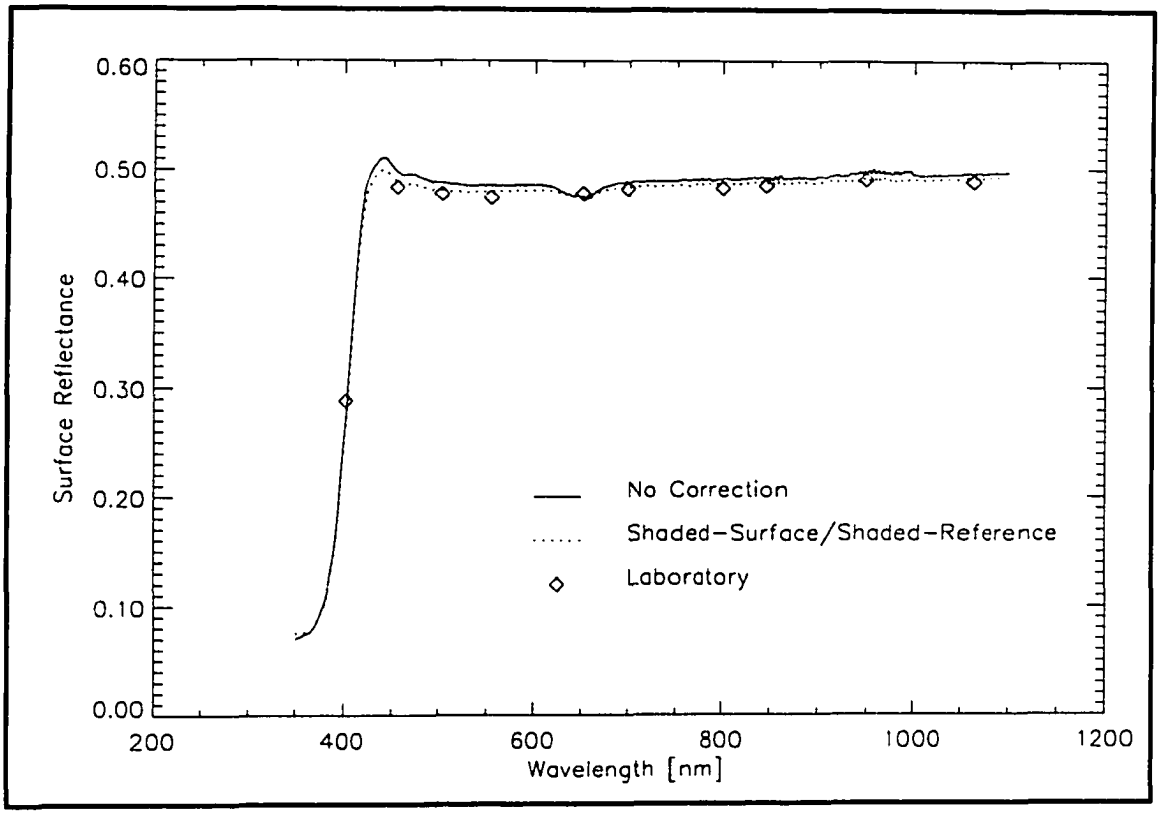


**Figure 4.4** Reflectance values for the 48% reflectance tarpaulin with a solar zenith angle of 40.1°.

wavelength in this band, the reflectance error of both methods changes sign, but the shaded-surface/shaded-reference method still has a smaller magnitude, as is shown in Figure 4.5. Comparing the ratio $L'_{diff}/L'_{total}$ and $L_{diff}/L_{total}$ it can be seen that there is a rise in the ratio measured over the panel in the range from 625 nm to 675 nm, but not over the tarpaulin. Further examination of the radiance show that the differences noted are due to changes in the reflected diffuse radiance through that range. Recent experiments comparing the results of several similar spectroradiometers indicate that the response of this instrument may be non-linear, which could explain this irregularity in the measured reflectances (Biggar, 2001).

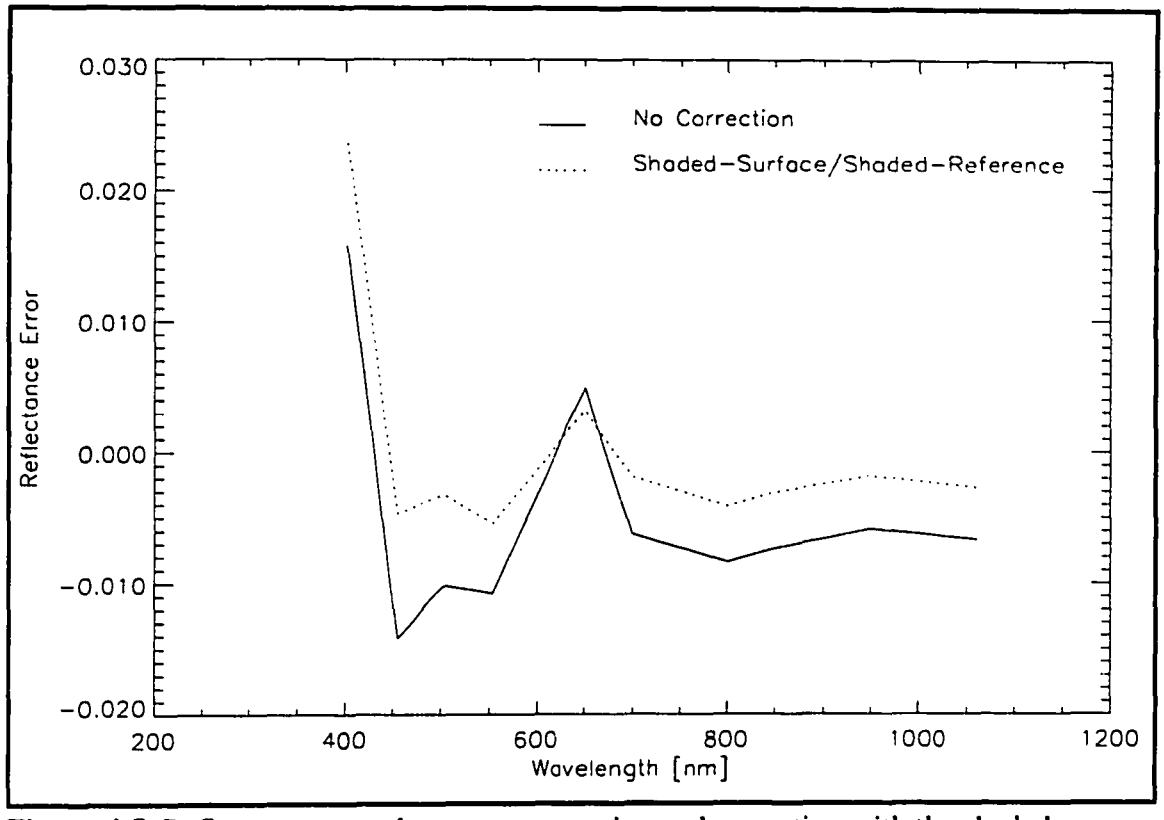


**Figure 4.5** Reflectance error due to not correcting and correcting with the shaded-surface/shaded reference method applied to the 48% reflectance tarpaulin at a solar zenith angle of 40.1°.

In general, the shaded-surface/shaded-reference method agreed with the laboratory measurements to within better than 0.01 reflectance units for the 8% and 48% tarpaulins and to within better than 0.02 reflectance units for the 2% tarpaulin. The exceptions to this included the error at 400 nm for the 48% tarpaulin mentioned above, and larger errors for the other two tarpaulins with occurred at 948 nm in the water vapor absorption band. The signals recorded for the shaded tarpaulins are very low to begin with, and so the large errors

in the water vapor band are expected due to small changes in the spectroradiometer's dark signal over the time of the measurements.

*Experimental setup for 3 March 2000*

The experimental set-up and procedure for 3 March 2000 was the same as for 3 July 2000 except for the following. The spectroradiometer used was an older model and its responsivity is less stable with time. Because of this 30 spectra were averaged for each file saved rather than 20, and a dark signal was measured before each unshaded radiance measurement. These dark signals are automatically subtracted from the data by the spectroradiometer's control software, and it is therefore difficult to quantify their effect.

The solar radiometer and barometric data were reduced to determine the atmospheric optical depths, Junge parameter, and ozone density, which were then used as inputs to the RTC and are listed in Table 4.1. The RTC assumes an infinite, homogenous, plane-parallel surface and the tarpaulins are only 61 cm to a side. Thus, the surface reflectance used as input to the RTC was taken as the measured surface reflectance of the gravel surrounding the experiment rather than the tarpaulins themselves.

| Parameter | Value |
|---|---|
| Junge Parameter | 3.4010 |
| Aerosol Index of Refraction | $1.44 + 0.005i$ |
| Aerosol Radius Range [μm] | [0.01, 5.01] @ 0.01 |
| View Angles ($\theta$,$\phi$) [degree] | (0.0, 0.0) |
| Altitude Range [km] | [0.747, 50.0] |
| Pressure [mbar] | 929.00 |
| Ozone Number Density [$cm^{-3}$] | 0.354 |
| Aerosol Optical Depth @ 0.55 μm | 0.0548 |

**Table 4.1** Atmospheric properties for the RTC for 3 March 2000.

*Results for 3 March 2000*

The importance of the orientation of the reflectance tarpaulins was not discovered until after this experiment was performed and sufficient care was not taken to record the orientation of the tarpaulins. Therefore, it is not possible to compare the results reliably with the laboratory data. However, since the shaded-surface/shaded-reference method has been shown to accurately retrieve the desired nadir-view reflectance the results of the other two models will be compared with shaded-surface/shaded-reference results.

Figure 4.6 is a plot of the reflectance error for both correction methods and for not correcting for the 48% reflectance tarpaulin. From this plot it is obvious that the shaded-reference method is significantly over correcting. One explanation for this is that the area in which the experiment was performed has many buildings and other obstructions surrounding it. Thus the $L_{sky}$ incident on the reference when $L'_{diff}$ is measured is very different from the modeled $L_{sky}$ used to calculate $L_{diff}$. The RTC-only method uses the modeled $L_{sky}$ for the calculation of both $L'_{diff}$ and $L_{diff}$. The presence of an obstruction can be simulated by changing values of the modeled $L_{sky}$ and observing the difference retrieved reflectances. The change in the shaded-reference method is shown to be two orders of magnitude greater than the change in the RTC-only method. This is because the correction performed in the RTC-only method will contain the error due to the obstruction in both the numerator and the denominator of the correction factor, while the shaded-reference method is attempting to use modeled and measured data together. Therefore, the RTC-only method will be more reliable for any case where there are differences between the actual and modeled $L_{sky}$.

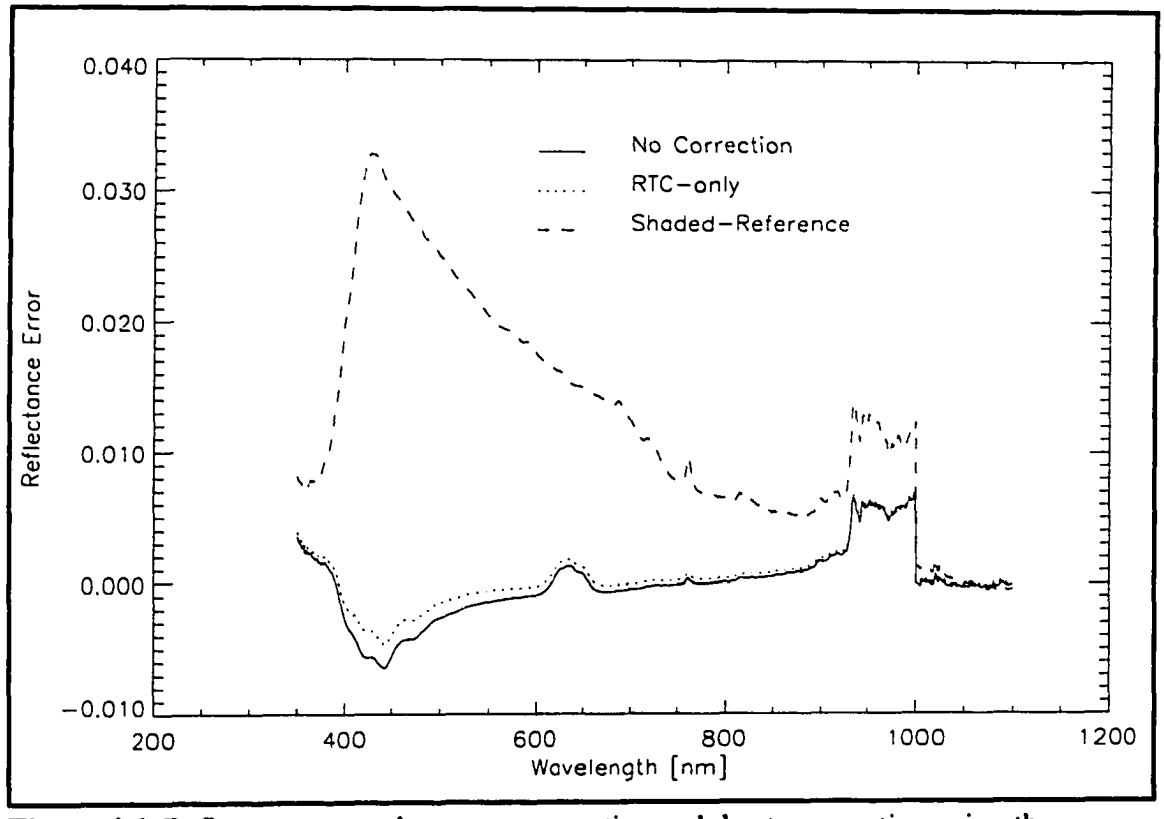


**Figure 4.6** Reflectance error due to not correcting and due to correcting using the shaded-reference and RTC-only methods for the 48% reflectance tarpaulin on 3 March 2000.

The sudden change in all three errors below 400 nm corresponds with the rapid decrease in the reflectance of the tarpaulin. Figure 4.7 plots the measured BRF for the 48% tarpaulin with the creases aligned vertically at 554 nm and also the values measured at 402 nm scaled such that the BRF's are the same at 45°. From this plot it can be seen that the shape of the BRF curve is not constant with wavelength. If the shape of the BRF continues to change for wavelengths less than 400 nm, this could explain the unexpected changes seen in Figure 4.6. At wavelengths greater than 400 nm the RTC-only method produces a surface

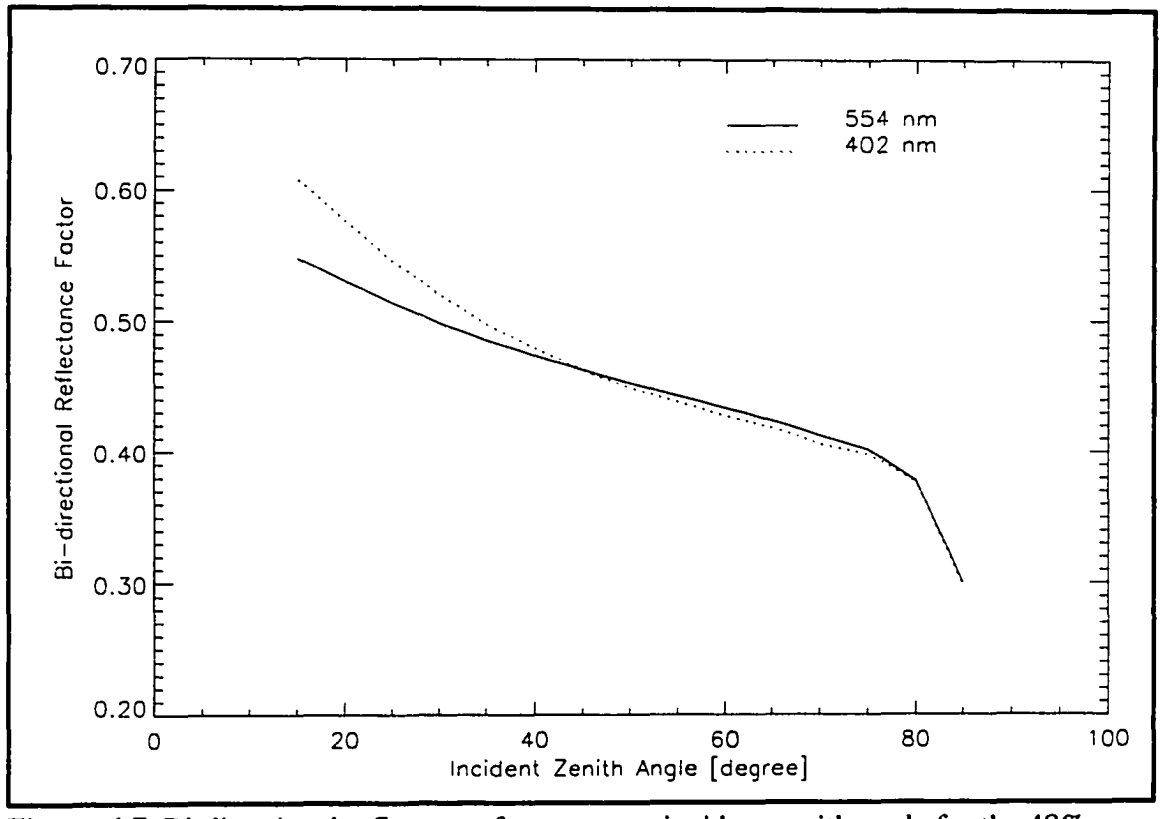


**Figure 4.7** Bi-directional reflectance factor versus incident zenith angle for the 48% reflectance tarpaulin at 402 nm and 554 nm.

reflectance value which is closer to that of the shaded-surface/shaded reference method, despite the significant differences between the actual and the modeled values for $L_{sky}$.

The variation in the reflectance near 650 nm discussed in the previous section is visible in the reflectance differences plotted in Figure 4.6. The effect is evident in the results for not correcting and correcting using the RTC-only method, but not in the results of the shaded-reference method. Because the anomaly is observed when $L'_{diff}$ is ignored or modeled, but not when $L'_{diff}$ is measured, its cause is assumed to be related to the reference measurements, which is consistent with the spectroradiometer's response being non-linear.

Also of note in Figure 4.6 is the small peak in the reflectance difference due to oxygen absorption near 760 nm for all three methods. In Chapter 3 is was shown that gaseous absorption causes the relative distribution of the diffuse radiance to change. This shift in the diffuse radiance field in turn causes changes in the magnitude of the error introduced by neglecting the reflected diffuse radiance. Just as in the case of the obstructions in the experiment area, the peak is most noticeable in the shaded-reference method because the measured $L'_{diff}$ includes the oxygen absorption while the modeled $L_{diff}$ does not.

The results of applying the shaded-reference and RTC-only methods to the 8% and 2% tarpaulins were similar to that seen for the 48% tarpaulin, although the change in the error below 400 nm is less drastic. Figure 4.8 and 4.9 plot the reflectance errors for the 8% and 2% tarpaulins, respectively. The discontinuity in Figure 4.9 around 948 nm is caused by the extremely small signals present in the water vapor absorption band. The signals are so small that small changes in the spectroradiometer's dark signal or in the water vapor amount between measurements cause large changes in the retrieved reflectance.

*Conclusions*

The shaded-surface/shaded-reference method is a reliable and robust method for retrieving the nadir-view reflectance, even in somewhat cloudy or otherwise non-ideal situations. For these conditions the shaded-reference method is not an appropriate choice, because the differences between the actual and modeled $L_{sky}$ are too great. The RTC-only method produces a reflectance which is improved compared to not correcting, and is far less sensitive to variations in the modeled $L_{sky}$ than the shaded-reference method.

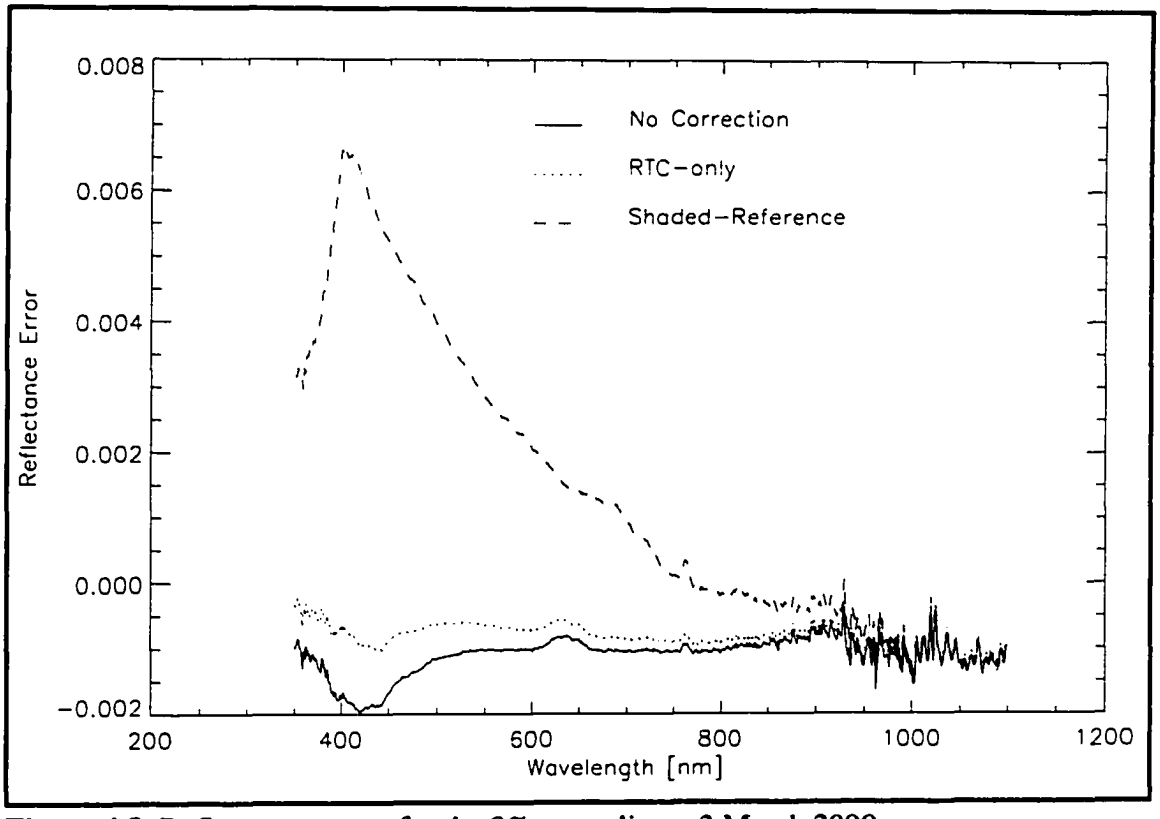


**Figure 4.8** Reflectance errors for the 8% tarpaulin on 3 March 2000.

### Measurements at White Sands Missile Range, 28 October 1999

On 28 October 1999 data were collected at White Sands Missile Range (WSMR) in Alamagordo, New Mexico in order to examine the application of the diffuse correction methods in typical field conditions. Unshaded and shaded upwelling radiance measurements were collected over a calibrated reference panel and over various portions of the surface. Solar radiometer data were not collected on the 28th, however these data were collected on the 29th and the atmospheric conditions appeared largely similar on the two days. The results in Chapter 3 demonstrate that small errors in the inputs to the radiative transfer code do not cause significant errors in the diffuse correction methods, and so the solar radiometer data

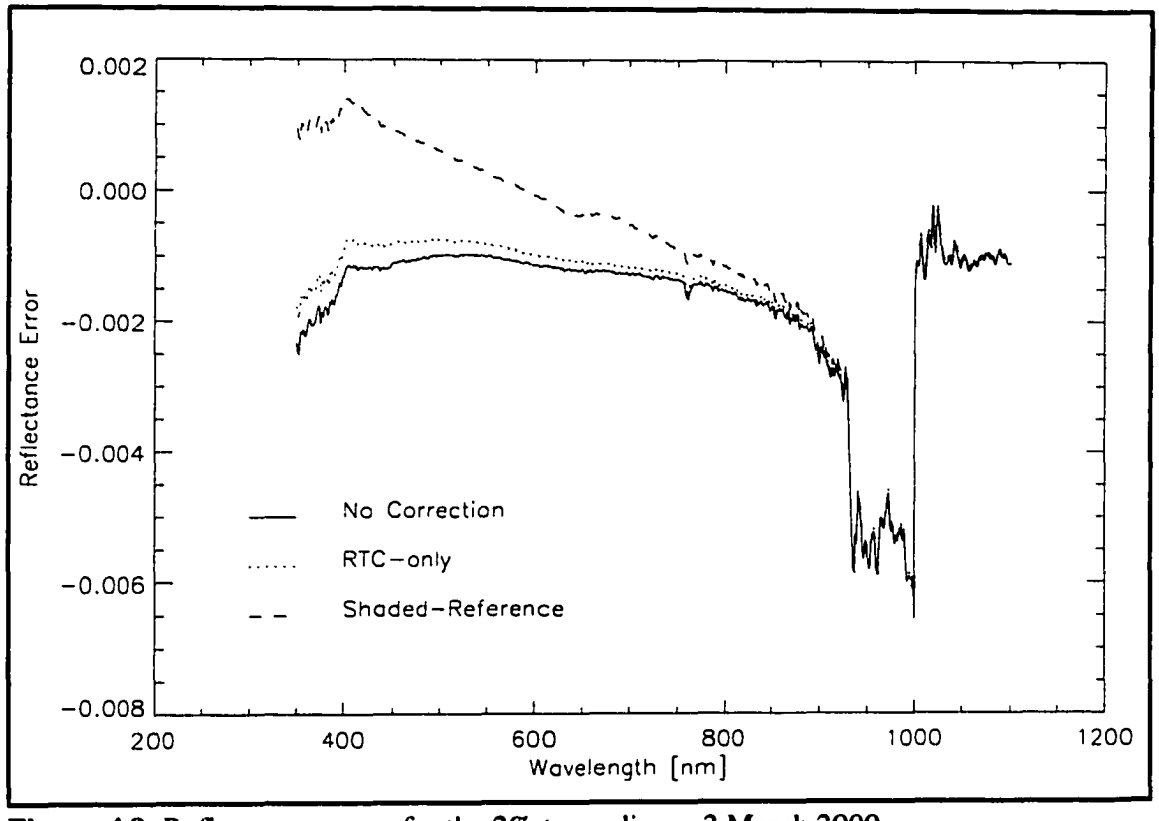


**Figure 4.9** Reflectance errors for the 2% tarpaulin on 3 March 2000.

from the 29th was used in the application of the shaded-reference and RTC-only methods. The BRF used for the surface was measured using the RSG's BRF camera system, Nandy 2000.

As in the case of the reflectance tarpaulins on 3 July 2000, the true surface reflectance of the surface was unknown, and so the results of the uncorrected, shaded-reference, and RTC-only methods are compared to the values calculated using the shaded-surface/shaded-reference method. Figure 4.10 is a plot of the surface reflectance as calculated using each of the methods.

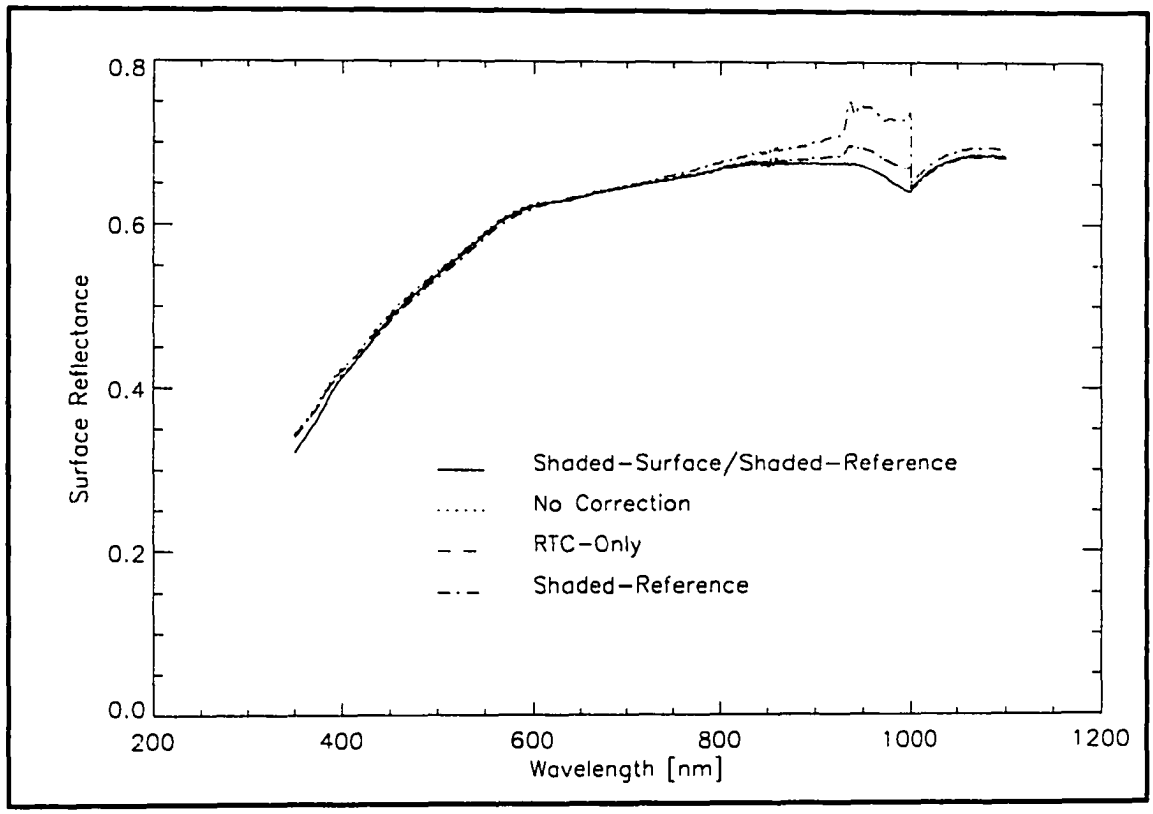


**Figure 4.10** Surface reflectance of White Sands Missile Range on 28 October 1999.

Figure 4.11 is a plot of the difference between the shaded-surface/shaded-reference reflectance and the reflectance calculated using the other three methods. The results of the shaded-reference method are significantly better for these data because there are fewer obstructions to the diffuse radiance field near the site at WSMR. However, the difficulty of using modeled and measured radiances is still apparent from the rapid change in the reflectance differences starting at 600 nm.

The RTC-only method produces reflectance values which are consistently closer to the shaded-surface/shaded-reference method than those calculated without correction. Both

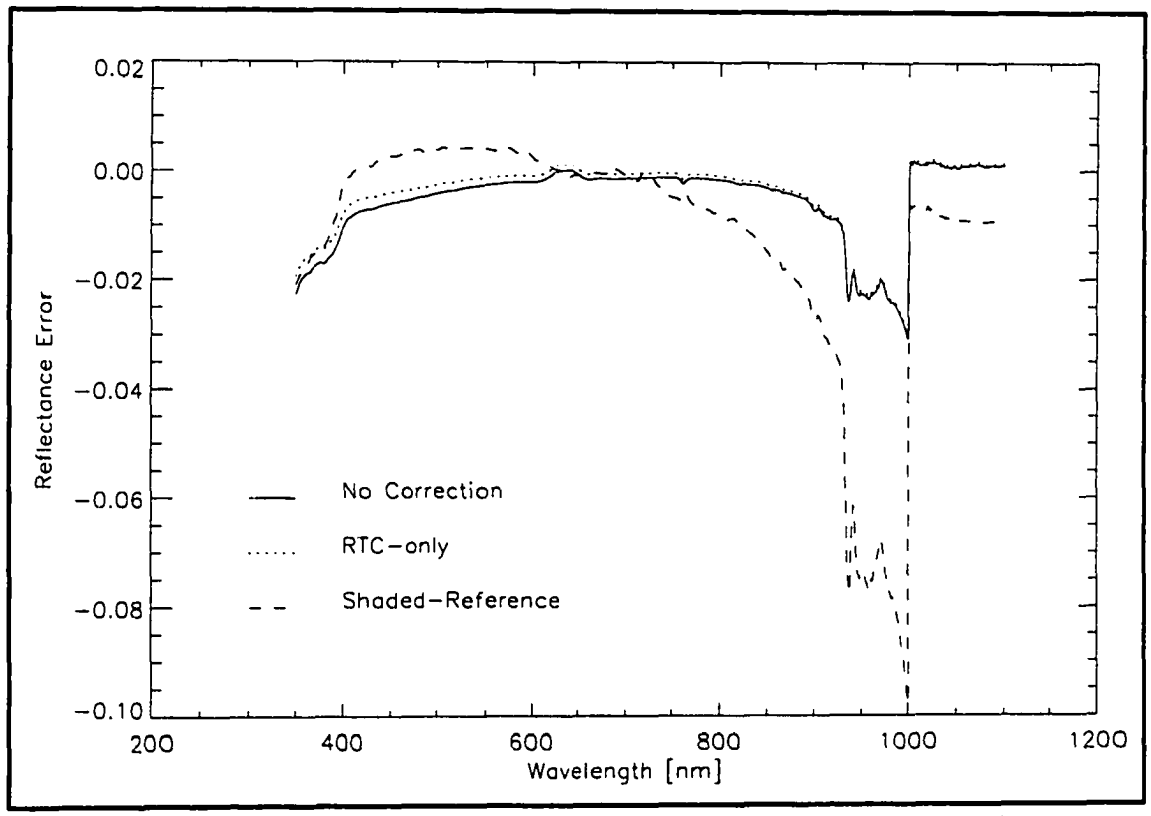


**Figure 4.11** Reflectance difference for diffuse correction methods referred to the reflectance calculated using the shaded-surface/shaded-reference method.

the RTC-only and uncorrected results demonstrate the anomalous reflectance near 650 nm which was first noticed in the results from 7 July 2000.

The shaded-surface/shaded-reference method is accurate and does not require any knowledge of $BRF_{surf}$ or $L_{sky}$, but because of the additional time and effort involved it will not normally be practical to apply it. The data needed for the shaded-reference and RTC-only methods can be collected within a reasonable time, but both methods need estimates for both $BRF_{surf}$ and $L_{sky}$. In fact, because the shaded-reference methods attempts to utilize both the measured value of $L'_{diff}$ and the modeled value of $L_{diff}$, the differences between the modeled and actual $L_{sky}$ cause errors in the retrieved surface reflectance. The results of the

RTC-only method have been shown to be an improvement over not correcting in cases where the shape of the surface BRF is moderately well known. Further, since application of this method does not require data to be collected in beyond that which is normally collected for the RSG's vicarious calibration efforts, the RTC-only method should be applied to field reflectance measurements.

# CHAPTER 5

# CONCLUSIONS AND RECOMMENDATIONS

One major source of error in the vicarious calibration methods employed by the RSG is the surface reflection measurements. In previous chapters, two contributors to the surface reflection error have been addressed, the spectral interpolation of laboratory data and the contribution of diffuse radiance on field measurements. The spectral interpolation was modified to use the hemispherical reflectance rather than a polynomial, and three methods were developed to remove the reflected radiance due to diffuse light. In this chapter the relative merits and problems with each method will be discussed, as well as recommendations for future improvements.

## Conclusions

### *Interpolation of the laboratory reflectance data*

The spectral interpolation of the laboratory reflectance measurements can more accurately be performed using the hemispherical reflectance rather than a polynomial. The measured hemispherical reflectances can then be fit to the discrete data from the black lab according to

$$\rho_{interpolated}(\lambda) = (b+m\lambda)\rho_{hemispheric}(\lambda) \qquad 5.1$$

where b and m are solved for to produce a least squares fit to the discrete data. Using this method provides a better fit to the discrete data, especially near the absorption feature in the short-wave infrared.

The angular interpolation is performed using a polynomial which has been constrained so that the coefficient of the first order term is zero. This constraint prevents the polynomial from extrapolating a specular peak in the reference panel's BRF. Because changing the polynomial order used for the angular interpolation does not significantly change the interpolated reflectance it is not necessary to change this method to a physically based interpolation.

*Shaded-surface/shaded-reference method*

Using the shaded-surface/shaded-reference method upwelling radiances are measured with and without the parasol blocking the directly transmitted solar irradiance from both the reference panel ($L'_{diff}$, $L'_{total}$) and the surface ($L_{diff}$, $L_{total}$). With these data $L_{sol}$ and $L'_{sol}$ can be calculated and the desired nadir-view reflectance can be determined.

The shaded surface method is the most accurate of the three methods because it does not rely on knowledge of the surface BRF or modeling of the at surface radiance field. The major sources of error for this method are the calibration of the reference and the stability of the spectroradiometer, and this method will typically improve the accuracy of reflectance measurements at the RSG's calibration sites by 0.005 to 0.01 reflectance units. Since this method requires that the person collecting the data stop in each pixel to measure $L_{diff}$, the time needed to collect the data from a calibration site will be at least doubled, and an additional person is required to hold the parasol. Further, there is the possibility that the weight of the parasol will cause it to damage the surface of the site while it is being used for $L_{diff}$ measurements. These issues make the shaded-surface/shaded-reference method

impractical for standard field measurements, though not impossible if the additional accuracy is needed.

*Shaded-reference method*

The shaded-reference method requires that $L_{total}$, $L'_{total}$, and $L'_{diff}$ be measured and that the atmosphere be characterized to determine the inputs for the RTC. Using the RTC output and an estimate of $BRF_{surf}$, $L_{diff}$ is calculated based on the measured values of $L_{total}$. Since the modeled value for $L_{diff}$ includes all of $L_{sky}$, the measured value of $L'_{diff}$ is corrected for the scattered light which is blocked by the parasol. The surface reflectance is then calculated in the same manner as in the shaded-surface/shaded-reference method.

The additional data required to apply the shaded-reference method can be collected without significantly increasing the data collection time. However, because this method tries to model $L_{diff}$ while using a measured value for $L'_{diff}$ any differences between the actual and modeled sky radiance will cause large errors in the retrieved reflectance. This makes the method sensitive to features in the sky radiance which are not modeled by the RTC, such as clouds or nearby buildings. The method is also sensitive to changes in the responsivity of the spectroradiometer while it is warming up. This limits the application of the method to remote sites on cloudless days when the spectroradiometer has been given sufficient time to warm up.

*RTC-only method*

The RTC-only method does not require any data be collected in the field beyond what is normally collected for the RSG's vicarious calibrations, which makes this method suitable for applying to archived as well as newly acquired data sets. This method uses the RTC

output and an assumed $BRF_{surf}$ to estimate the expected errors in the uncorrected reflectance, and then adjusts the uncorrected reflectance by that amount.

The accuracy of the RTC-only method is largely determined by the accuracy of the shape of the assumed $BRF_{surf}$. In order to maintain an accuracy of 2% reflectance units biases in the values of $BRF_{surf}$ at large angles must be less than 25% for solar zenith angles between 35° and 60°, with greater accuracy needed for solar angles less than 35°. Current work on the measurement of the surface BRF indicates that this level of accuracy is possible (Nandy, 2000). For cases where the BRF is known to this accuracy, this method has been shown to improve the accuracy of the reflectance measurements by approximately 0.003 reflectance units. Therefore, it is worthwhile to apply the RTC-only method to field reflectance data where a suitable $BRF_{surf}$ is available.

Table 5.1 summarizes the expected improvement from using the different diffuse correction methods, along with their advantages and disadvantages.

**Recommendations**

The RSG has several other instruments whose data could be incorporated to improve the accuracy of the diffuse corrections. Since the dominant source of error in both the RTC-only method is the unknown surface BRF, the BRF camera will contribute dramatically to improvements in the corrections. This instrument allows more frequent measurements of the surface BRF, including data collected at the solar angle at which the surface reflectance data is collected. Also, since the data will be on the same trip differences due to rain fall or other meteorological effects will be avoided. Further, since the BRF camera is based on a two dimensional CCD array, it would be possible to determine the BRF as a function of both $\theta$

| Correction Method | Advantages | Disadvantages | Expected Improvement |
|---|---|---|---|
| RTC-Only | No additional data needs to be collected | Requires an estimate of the surface BRF<br>Reflectance processing takes longer | 0.003 |
| Shaded-Reference | Minimal additional data required<br>$L'_{diff}$ is measured rather than modeled | Requires an estimate of the surface BRF<br>Strong sensitivity to differences in the actual and modeled diffuse radiance | Depends on the conditions |
| Shaded-Surface/Shaded-Reference | No knowledge of the surface BRF is needed<br>Both $L_{diff}$ and $L'_{diff}$ are measured | Data collection time is doubled<br>And additional person is required to carry the parasol<br>Possibility of damage to the site | 0.005 - 0.01 |

**Table 5.1** Comparison of diffuse correction methods.

and $\phi$. Since the modeled radiance output by the RTC is already a function of both variables, the modification of the correction methods to include a two dimensional BRF would be straight forward.

During field measurements the RSG uses the all-sky camera to record the cloud cover at the time of the overpass. The all-sky camera is a film based camera with a 180° FOV fisheye lens, which takes a picture of the entire sky. If clouds are blocking either the sun or the satellite view at the time of overpass, the data are unusable, but calibrations are performed when clouds are present which do not obstruct the solar or view directions. The

pictures from the all-sky camera could be digitized and the higher radiances due to the clouds could be incorporated into the diffuse field predicted by the RTC. Either the all-sky camera or the BRF camera could be used to take an image of the sky in cloudless conditions and these data could be used to further constrain the distribution of $L_{sky}$, as well.

Another instrument which will benefit the diffuse corrections is the Diffuse-to-Global meter. This instrument uses a carefully leveled integrating sphere with an automated occulting disk to measure both the total downwelling irradiance and diffuse downwelling irradiance. These data are used to further constrain the aerosol model used by the RTC and could also be used to better understand the differences in the magnitudes of the actual and modeled diffuse radiances, and thereby improve the accuracy of the shaded-reference method.

The shaded-surface/shaded-reference method is accurate and robust, and does not require knowledge of $BRF_{surf}$. The RTC-only does not require additional data to be collected and can therefore be applied to archived data sets. Also the recommendations in this chapter are likely to improve the accuracy of the RTC-only and shaded-reference methods. Correcting for the contributions due to diffuse radiance is a worthwhile improvement to the measurement of surface reflectance in the field and this work describes methods which can be used to perform this correction.

# APPENDIX A

# LABORATORY REFLECTANCE FACTOR MEASUREMENTS

The Remote Sensing Group (RSG) measures the surface reflectance of its calibration sites by comparing the measured upwelling radiance from the site to that from a reference panel with known direction reflectance properties. The procedure the RSG uses for measuring the bi-directional reflectance factor (BRF) of the reference panel in the laboratory (Biggar, 1988) will be presented in this appendix.

## Equipment and Setup

There are three central components to the experimental setup; the sample holder, the radiometer, and the source. The sample holder has three degrees of freedom for positioning the sample with respect to the source and the radiometer. There are two rotation stages which allow the incident and view zenith angle to be set independently within the plane defined by the incident illumination and the sample normal. A third rotation allows the sample to be tilted such that the sample normal is no longer contained in the principle plane. The sample is held such that its front surface is coincident with the vertical rotation axis of the stages, and the setup is aligned by mounting a mirror to the holder and using laser to define the optical axis through the source.

There are multiply interference filter-based radiometers used in the laboratory to cover the visible and near infrared and the shortwave infrared spectrums. The appropriate radiometer is mounted on an L-shaped arm which is attached between two of the rotations stages of the sample holder, and it is aligned to the optical axis.

The source used is a 1000 W quartz halogen lamp operated in a constant current mode at 8 amps. The lamp is located in an adjacent room to the sample holder and radiometer, and illuminates the sample through a 5 cm aperture. This aperture limits the illumination to the center of the sample which reduces stray reflectances. Figure A.1 is a diagram of the laboratory layout. The rotation stages of the sample holder and the mount for the lamp are attached to a single table which extends through the wall between the two rooms. And all exposed surfaces in the sample room are blacked in order to reduce the affects of stray light.

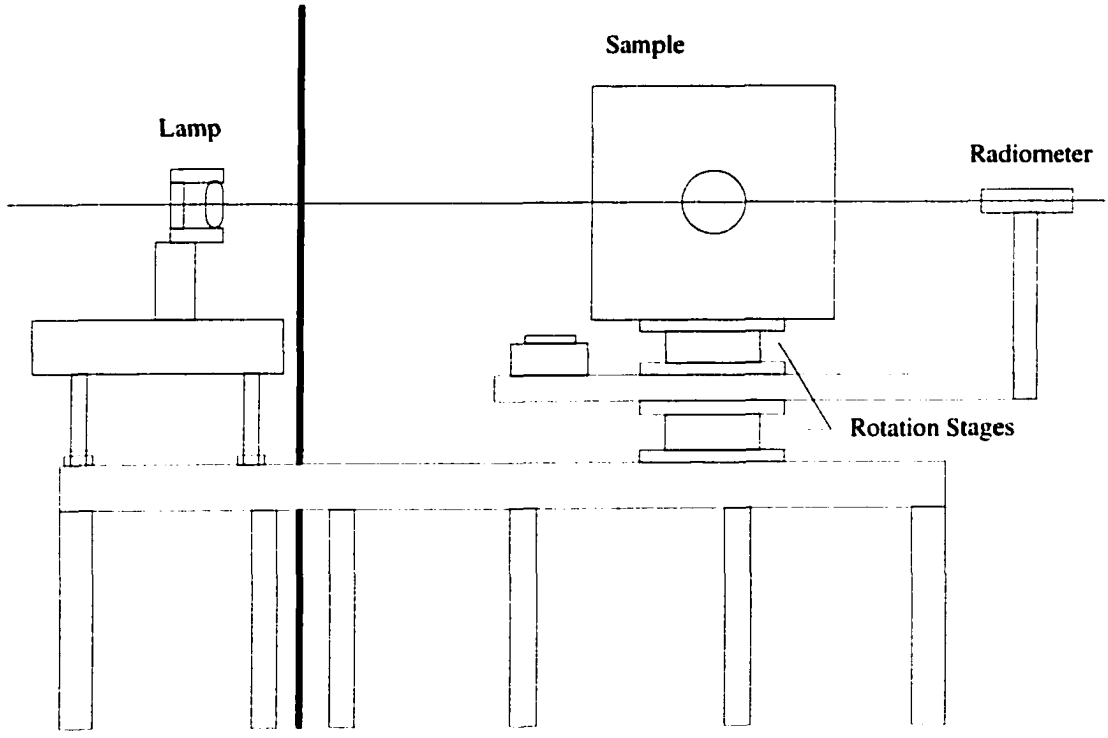


**Figure A.1** Laboratory set up for BRF measurements.

**PTFE Reference**

The laboratory measurements are made in reference to a pressed sample of polytetraflouroethylene powder which is prepared according to the procedure prescribed by NIST (Weidner et al, 1985). Halon, the brand of PTFE used by Weidner, is no longer available but it has been shown that Algoflon can be used in its place (Spyak and Lansard, 1997). The sample therefore has a known hemispherical reflectance.

**Method of Reflectance Factor Retrieval For PTFE Sample**

The hemispherical reflectance factor for a normal incidence angle (HRF(0°)) can be calculated as

$$HRF(0°) = \frac{\int_0^{\frac{\pi}{2}} BRF(0°;\theta_{view})\cos\theta_{view}\sin\theta_{view}2\pi d\theta_{view}}{\int_0^{\frac{\pi}{2}} \cos\theta_{view}\sin\theta_{view}2\pi d\theta_{view}} \qquad \text{A.1}$$

where $BRF(0°;\theta_{view})$ is the bi-directional reflectance factor for a view angle of $\theta_{view}$ and a normal incident angle. Dividing by $BRF(0°;45°)$ gives

$$\frac{HRF(0°)}{BRF(0°;45°)} = 2\int_0^{\frac{\pi}{2}} \frac{BRF(0°;\theta_{view})}{BRF(0°;45°)}\cos\theta_{view}\sin\theta_{view}d\theta_{view} \qquad \text{A.2}$$

when the denominator of Equation A.1 is evaluated and like terms are canceled. Substituting in measurable quantities

$$\frac{HRF(0°)}{BRF(0°;45°)} = 2\int_0^{\pi/2} B(0°;\theta_{view})\cos\theta_{view}\sin\theta_{view}\,d\theta_{view} \qquad \text{A.3}$$

where

$$B(0°;\theta_{view}) = \frac{L(0°;\theta_{view})/\cos\theta_{view}}{L(0°;45°)/\cos(45°)} \qquad \text{A.4}$$

and L is the reflected radiance from the sample.

$B(0°;\theta_{view})$ can then be fit to a 5th order polynomial in $\theta_{view}$

$$B(0°;\theta_{view}) = \sum_{i=0}^{5} b_i \theta^i_{view} \quad . \qquad \text{A.5}$$

Substituting Equation A.5 into Equation A.3 gives

$$\frac{HRF(0°)}{BRF(0°;45°)} = 2\sum_{i=0}^{5} b_i I_i \qquad \text{A.6}$$

where

$$I_i = \int_0^{\frac{\pi}{2}} \theta^i_{view}\cos\theta_{view}\sin\theta_{view}\,d\theta_{view} \qquad \text{A.7}$$

which can be solved analytically.

Using measurements to solve for the coefficients in Equation A.5 allows Equation A.6 to be solved for BRF(0°;45°) by assuming that the HRF(0°) does not vary significantly from HRF(6°). And now $BRF(0°;\theta_{view})$ is given by

$$BRF(0°;\theta_{view}) = BRF(0°;45°) * B(0°;\theta_{view}) \quad . \qquad \text{A.8}$$

**Laboratory Measurements**

The laboratory data is collected with the radiometer fixed normal to the sample, while the stages are rotated collect at different incidence angles. These data can be used with the above derivation because of the Helmholtz reciprocity principle which states

$$BRF(0°;\theta) = BRF(\theta;0°) \qquad \text{A.9}$$

or, that the direction the light is traveling does not affect the value of the reflectance. The data are collected for incident angles between 15° and 85° for the VNIR bands and between -10° and -75° for the SWIR. The size and shape of the SWIR radiometer dictates that it be rotated in the opposite sense of the VNIR, otherwise it would cast a shadow on the sample for small incident angles. For both cases, data are collected at intervals of 5° in incident angle.

The data are collected at 22 wavelengths which are listed in Table

| VNIR Wavelengths [nm] | SWIR Wavelengths [nm] |
|---|---|
| 402 | 747 |
| 455 | 869 |
| 503 | 940 |
| 554 | 1243 |
| 651 | 1380 |
| 699 | 1646 |
| 800 | 2134 |
| 846 | 2164 |
| 949 | 2207 |
| 1061 | 2262 |
| | 2332 |
| | 2403 |

**Table A.1** Center wavelengths [nm] measured in the laboratory.

A.1. The data are collected for each wavelength and incident angle by averaging 100 reading for the VNIR and 30 for the SWIR and subtracting off the dark signal. Assuming the radiometers are linear, these voltages can be used in place of radiances in Equation A.4, and the coefficients for $B(\theta_{inc};0°)$ can be found using a least squares fit.

Using the known hemispherical reflectance of pressed PTFE powders and the fitted coefficients for $B(\theta_{inc};0°)$, the value of $BRF(45°;0°)$ can be calculated from Equation A.6. The values of the BRF for other incident angles are then given as

$$BRF(\theta_{inc};0°) = BRF(45°;0°) * B(\theta_{inc};0°) \quad . \qquad \text{A.10}$$

The field reference is then measured in the same manner as the pressed PTFE sample. The BRF for a particular incident angle, $\theta_{inc}$, is then calculated by ratioing the voltages measured from the field reference to those from the PTFE sample and multiplying by the known BRF of the PTFE. These are the discrete data to which the angular and spectral interpolation of Chapter 2 are applied.

# REFERENCES

Biggar, S.F., 1990b, In-Flight Methods For Satellite Sensor Absolute Radiometric Calibration. *PhD Dissertation, University of Arizona*, 153 pp.

Biggar, S.F., Labed, J., Santer, R.P., Slater, P.N., Jackson, R.D., Moran, M.S., 1988, Laboratory calibration of field reflectance panels. *SPIE Proc.*, Vol. 924, pp. 232-240.

Biggar, S.F., Santer, R.P., Slater, P.N., 1990a, Irradiance-based calibration of imaging sensors. *International Geoscience and Remote Sensing Symposium*, College Park, Maryland, pp. 507-510.

Biggar, S.F., Slater, P.N., Gellman, D.I., 1994, Uncertainties in the In-Flight Calibration of Sensors with Reference to Measured Ground Sites in the 0.4-1.1μm Range. *Remote Sens. Environ.*, Vol. 48, pp. 245-252.

Biggar, S.F., Slater, P.N., Thome, K.J., Holmes, A.W., Barnes, R.A., 1997, The solar-based calibration experiment of SeaWiFS. *Presented at NEWRAD '97.*

Biggar, S.F., Slater, P.N., Thome, K.J., 1993, Preflight solar based calibration of SeaWiFS. *SPIE Proc.*, Vol. 1939, pp. 233-242.

Bohren, C.F. and Huffman, D.R., 1983, *Absorption and Scattering of Light by Small Particles*, John Wiley & Sons, Inc., New York, New York.

Bruegge, C., Duval, V., Chrien, N., Korechoff, R., 1995, MISR instrument development and test status. *Satellite Remote Sensing II, Proc. SPIE*, Vol. 2583.

Coulson, K.L., 1988, *Polarization and Intensity of Light in the Atmosphere*, A. DEEPAK Publishing, Hampton, Virginia.

Dinguirard, M., Mueller, J., Sirou, F., Tremas, T., 1998, Comparison of ScaRaB ground calibration in the short-wave and long-wave spectral domains. *Metrologia*, Vol. 35, pp. 597-601.

Dinguirard, M., Slater, P.N., 1999, Calibration of Space-Multispectral Imaging Sensors: A Review. *Remote Sens. Environ.*, Vol. 68, pp. 194-205.

Edlen, B., 1953, The dispersion of standard air. *J. Opt. Soc. Am.*, Vol 43, pp. 339-344.

Elterman, L., 1968, UV, Visible and IR Attenuation for Altitudes to 50 km. Report AFCRL-68-0153, Air Force Cambridge Research Laboratories, Bedford, MA, 49 pp.

REFERENCES – continued

Epema, G.F., 1991, Studies of Errors in Field Measurements of the Bidirectional Reflectance Factor. *Remote Sens. Environ.*, Vol. 35, pp. 37-49.

Gu, X., Guyot, G., 1993, Effect of Diffuse Irradiance on the Reflectance Factor of Reference Panels Under Field Conditions. *Remote Sens. Environ.*, Vol. 45, pp. 249-260.

Gustafson-Bold, C.L., Thome, K.J., 1996, Cross-Calibration of Two Small Footprint Sensors. *Presented at International Geoscience & Remote Sensing Symposium, Lincoln Nebraska*, pp. 1283-1285.

Herman B.M., Browning, S.R., 1965, A numerical solution to the equation of radiative transfer. *J. Atmos. Sci.*, Vol. 22, pp. 559-566.

Hovis, W.A., Knoll, J.S., Smith, G.R., 1985, Aircraft measurements for calibration of an orbiting spacecraft sensor. *Appl. Opt.*, Vol. 24, pp. 407-410.

Jackson, R.D., Clarke, T.R., Moran, M.S., 1992, Bidirectional Calibration Results for 11 Spectralon and 16 $BaSO_4$ Reference Reflectance Panels. *Remote Sens. Environ.*, Vol. 40, pp. 231-239.

Jackson, R.D., Moran, M.S., Slater, P.N., Biggar, S.F., 1987, Field Calibration of Reference Reflectance Panels. *Remote Sens. Environ.*, Vol. 22, pp. 145-158.

Kattawar, G.W., Plass, G.N., 1967, Electromagnetic Scattering from Absorbing Spheres. *Appl. Opt.*, Vol. 6, pp. 1377-1382.

Kieffer, H.H., Wildey, R.L., 1996, Establishing the moon as a spectral radiance standard. *J. Atmos. Ocean. Technol.*, Vol. 13, pp. 360-375.

Kimes, D.S., and Kirchner, J.A., 1982, Irradiance Measurement Errors Due to the Assumption of a Lambertian Reference Panel. *Remote Sens. Environ.*, Vol. 12, pp. 141-149.

Labsphere, Inc., 2000, Electronic Communication.

Liou, K., 1980, *An Introduction to Atmospheric Radiation*, Academic Press, Inc., Orlando, Florida.

Lyapustin, A.I., Privette, J.L., 1999, A new method of retrieving surface bidirectional reflectance from ground measurements: Atmospheric sensitivity study. *J. Geophys. Res.*, Vol. 104, pp. 6257-6268.

REFERENCES –continued

Martonchik, J.V., 1994, Retrieval of Surface Directional Reflectance Properties Using Ground Level Multiangle Measurements. *Remote Sens. Environ.*, Vol. 50, pp. 303-316.

Mueller, J., Stulhmann, R., Becker, R., Raschke, E., Monge, J.L., Burkert, P., 1996, Ground based calibration facility for the Scanner for Radiation Budget instrument in the solar spectral domain. *Metrologia*, Vol. 32, pp. 657-660.

Nandy, P., 2000, Personal Communication.

Ono, A., Sakuma, F., Arai, K., Yamaguchi, Y., Fujisada, H., Slater, P.N., Thome, K.J., Palluconi, F.D., Kieffer, H.H., 1996, Preflight and In-Flight Calibration Plan for ASTER. *J. Atmos. Oceanic Technol.*, Vol. 13, pp. 321-335.

Slater, P.N., Palmer, J.M., 1991, Solar-diffuser panel and ratioing radiometer approach to satellite sensor on-board calibration. *Proc. SPIE*, Vol. 1493-12.

Spyak, P.R., Lansard, C., 1997, Reflectance properties of pressed Algoflon F6: a replacement reflectance-standard material for Halon. *Appl. Opt.*, Vol. 36, pp. 2963-2970.

Thome, K.J., Crowther, B.G., Biggar, S.F., 1997, Reflectance- and Irradiance-based Calibration of Landsat-5 Thematic Mapper. *Canadian Journal of Remote Sensing*, Vol. 23, pp. 309-317.

USSA, 1962, U.S. Standard Atmosphere, 1962. Cat. No. NAS 1.2:At6/962. GPO, Washington, DC.

Walter-Shea, E.A., Hays, C.J., Mesarch, M.A., Jackson, R.D., 1993, An Improved Goniometer System for Calibrating Field Reference-Reflectance Panels. *Remote Sens. Environ.*, Vol. 43, pp. 131-138.

Weidner, V.R., Hsia, J.J, 1981, Reflection properties of pressed polytetrafluoroethylene powder. *J. Opt. Soc. Am.*, Vol. 71, pp. 856-861.